This pdf file contains all figure pages in the dissertation:

EXTENSION AND EXHUMATION OF THE HELLENIC FOREARC

AND

RADIATION DAMAGE IN ZIRCON

by

Antonios E. Marsellos

A Dissertation

Submitted to the University at Albany, State University of New York

in partial fulfillment of

the Requirements for the degree of

Doctor of Philosophy

College of Arts & Sciences

Department of Earth and Atmospheric Sciences

2008

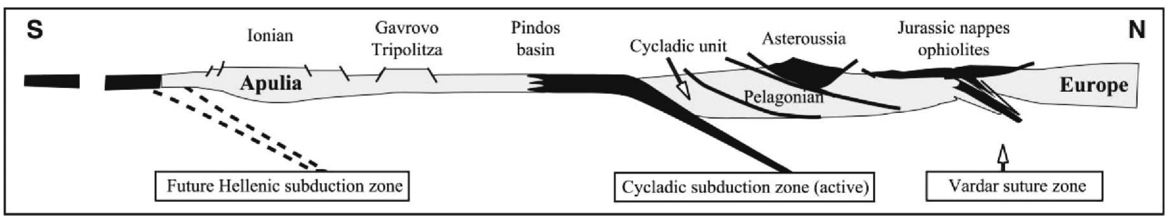

***Figure 1**:* Simplified cross-section of the Aegean domain in the <u>Late Cretaceous</u> (adapted from Bonneau, 1984; after Trotet et al., 2001) showing the ancient Cycladic subduction zone and the associated formation of the Cycladic unit.

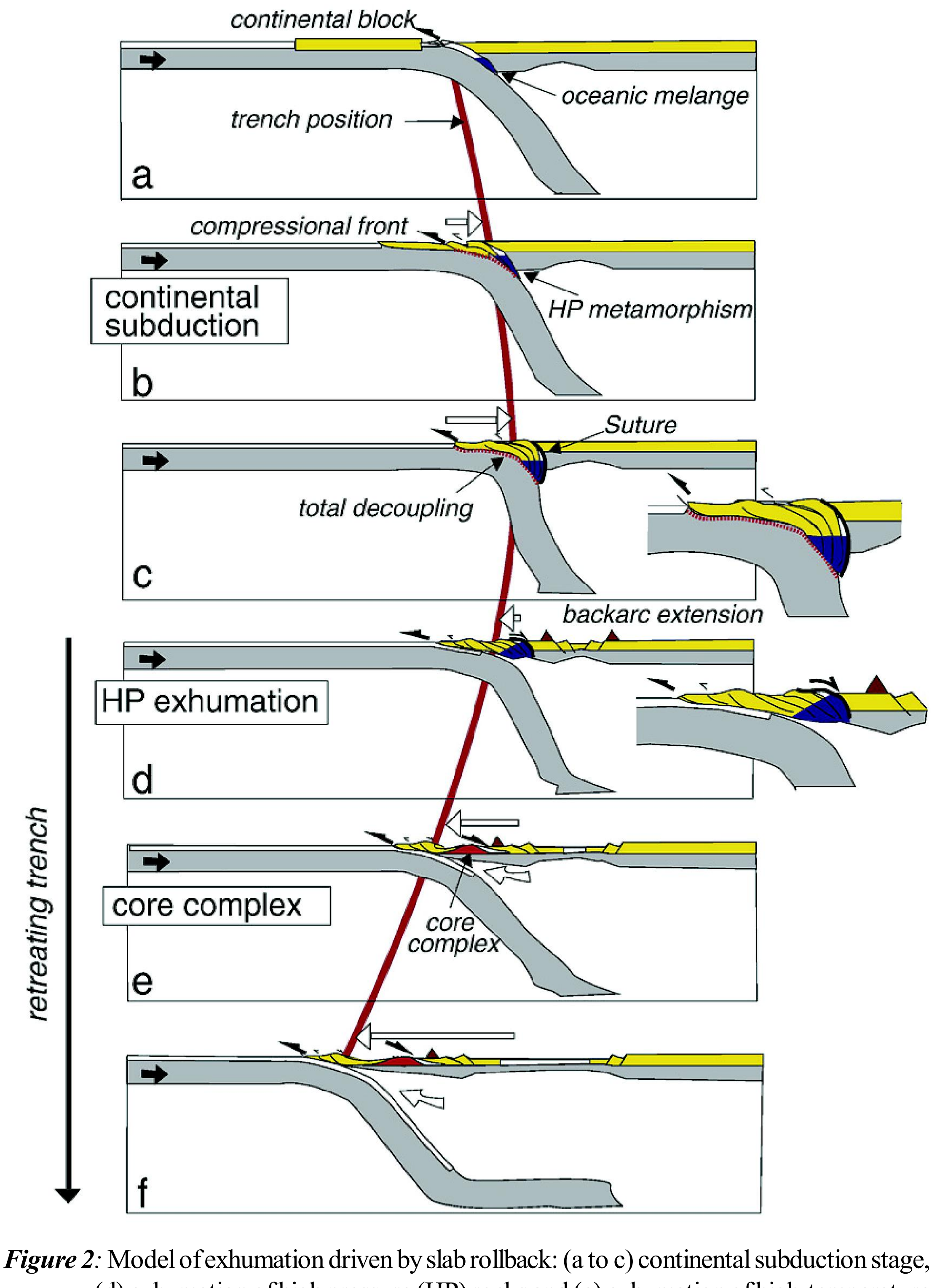

***Figure 2**:* Model of exhumation driven by slab rollback: (a to c) continental subduction stage, (d) exhumation of high pressure (HP) rocks and (e) exhumation of high-temperature (HT) rocks in core complex. The red line indicates trench retreat, while the white arrows indicate the trench advance (a to c) and retreat (d to f). Slab dip increases during subduction of the continental block (a to c), and then decreases during oceanic subduction (d to f), (Brun & Faccenna, 2008).

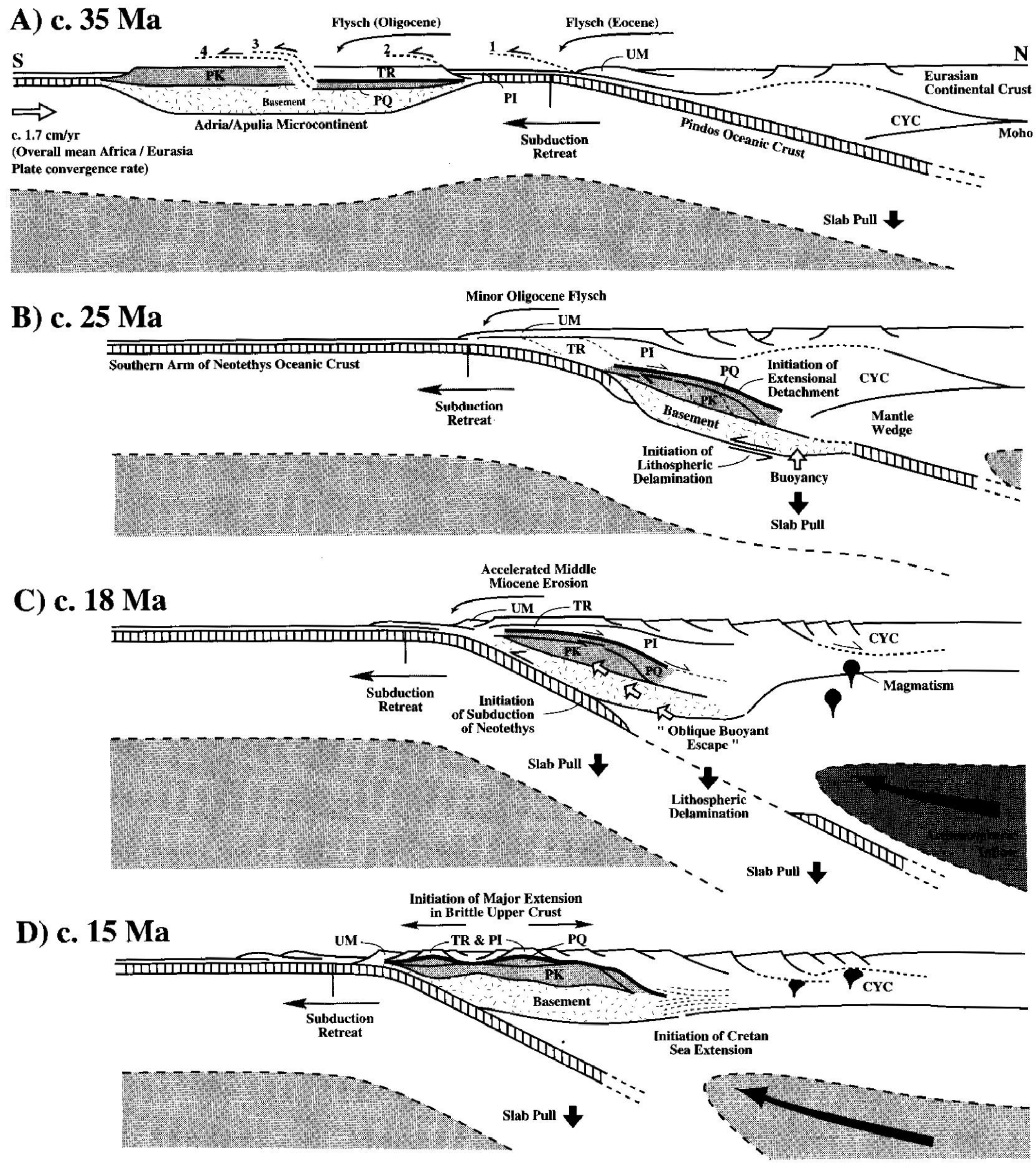

Figure 3: Schematic N-S cross-sections that illustrate the model of "oblique escape" for the late Eocene to mid-Miocene tectonic development of the Cretan segment of the Hellenic convergent boundary (Thomson et al., 1999). The age sequence of accretion of the different tectonic units of Crete is numbered in (a). The HP-LT lower plate rocks exposed at present on Crete are shaded. PK, Plattenkalk unit; PQ, Phyllite-Quartzite unit; TR, Tripolis unit; PI, Pindos unit; UM, Uppermost unit; CYC, present-day rocks of the Cyclades.

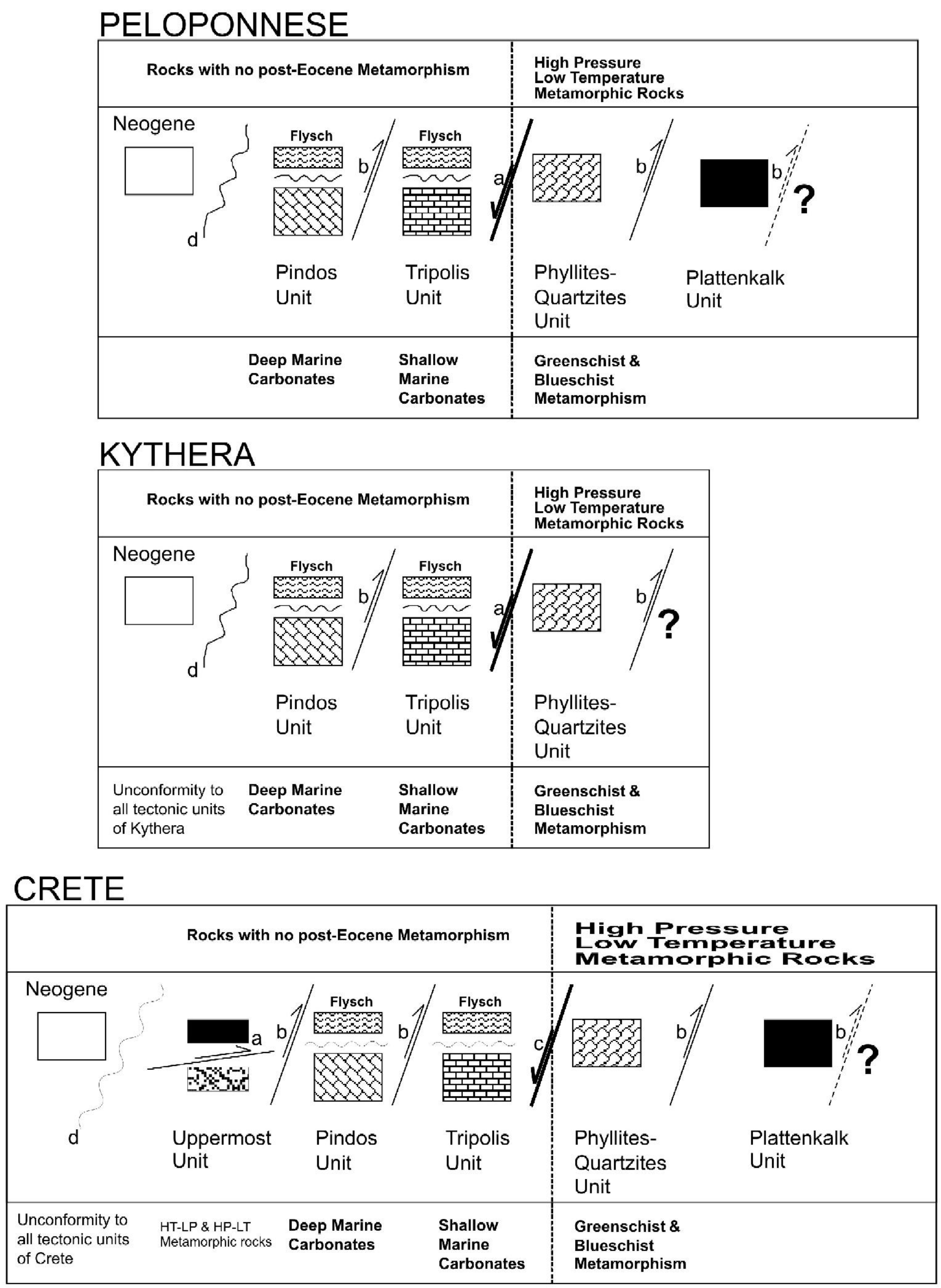

***Figure** 4:* Simplified tectonostratigraphy (after Thomson et al., 1998, 1999) for the central and western Hellenic Arc. a, thrust of post-Cretaceous age; b, major thrust contacts of Oligocene-Miocene age; c, extensional detachment of Miocene age, recognized by Jolivet et al., (1996) for Crete, by Marsellos & Kidd, (2006) for Kythera; d, Neogene sedimentary rocks of Tortonian age unconformably overlie all the tectonic units of Crete as well as those of Kythera.

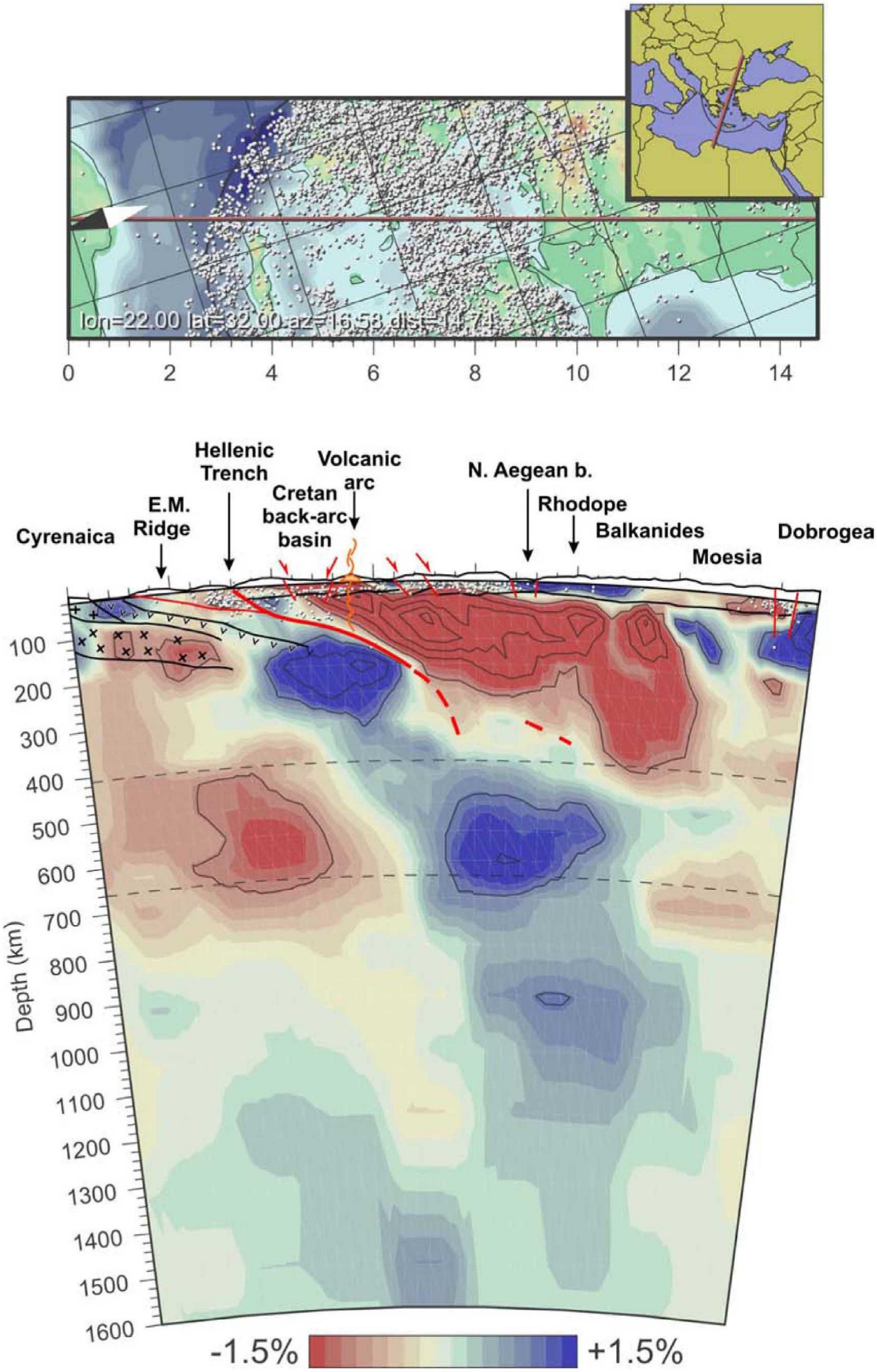

***Figure 5**:* Seismic-tomography in a NNE-SSW section through Greece, Transect VII, (Spakman, 1993).

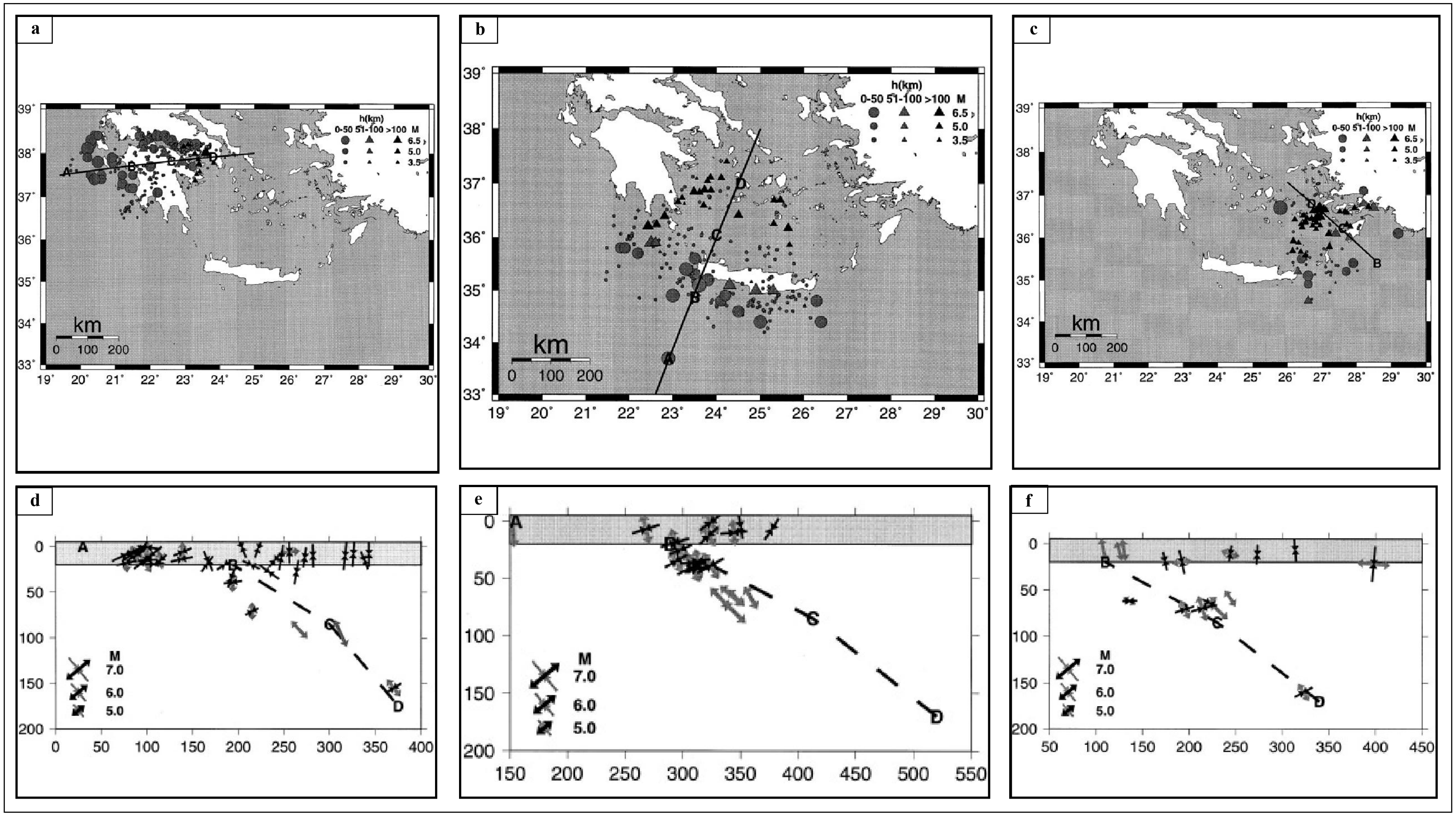

Figure 6 : (a-c) Shallow and deep parts of the subduction zone show 30 and 45 degree dips respectively. Maps with section locations, and (d-f) sketch sections of the Hellenic arc and the subduction zone through the Ionian Islands (western part), western Crete (central part) and Rhodes (eastern part). Stress field along the same cross-sections shown by conventional symbols. Extension occurs parallel to the dip of the Wadati-Benioff zone in all cross-sections at depths of more than 50-60km (from Papazachos, 2000).

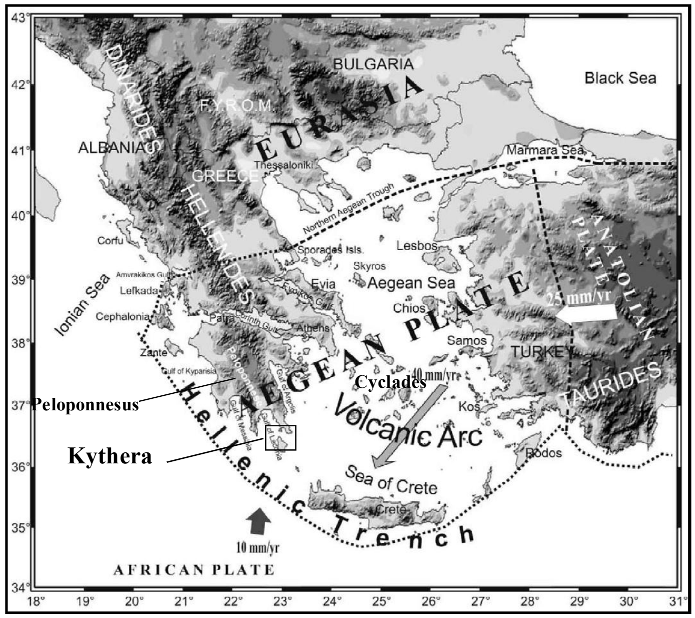

Figure 7: Location map of the Aegean Sea and the surrounding lands. The dashed line indicates the boundaries of the Aegean plate and the arrows indicate the motion of the plates relative to Eurasia (Anastasia Kiratzi et al., 2003).

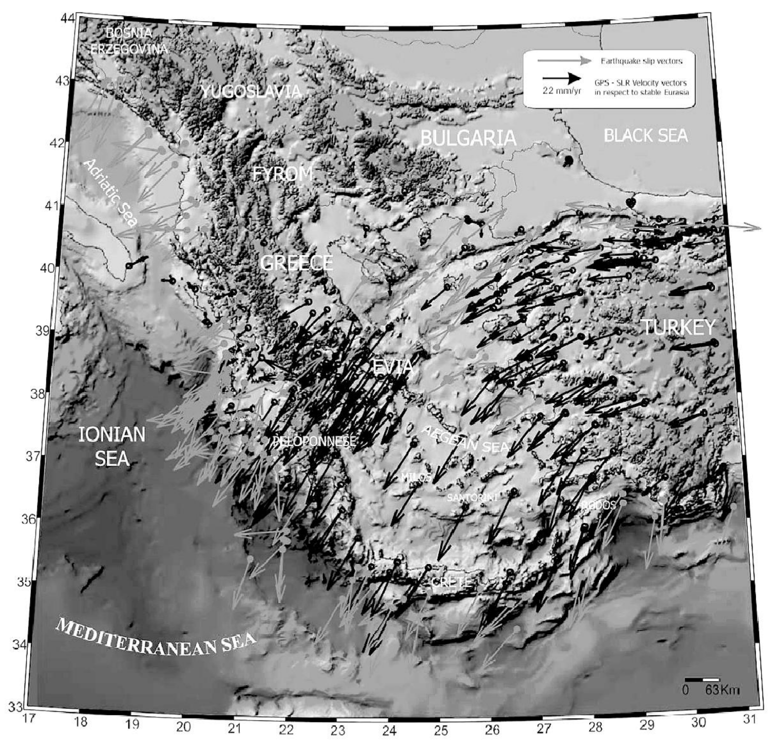

Figure 8: A compiled figure (after Kiratzi et al., 2003) shows comparison of earthquake slip vectors and of velocity vectors obtained from GPS and SLR measurement in respect to Eurasia (data from Oral, 1994; Reilinger et al., 1997; Clarke et al., 1998; Cocard et al., 1999; McClusky et al., 2000). Earthquake slip vectors represent movement of the hanging wall relative to the footwall (from Louvari, 2000).

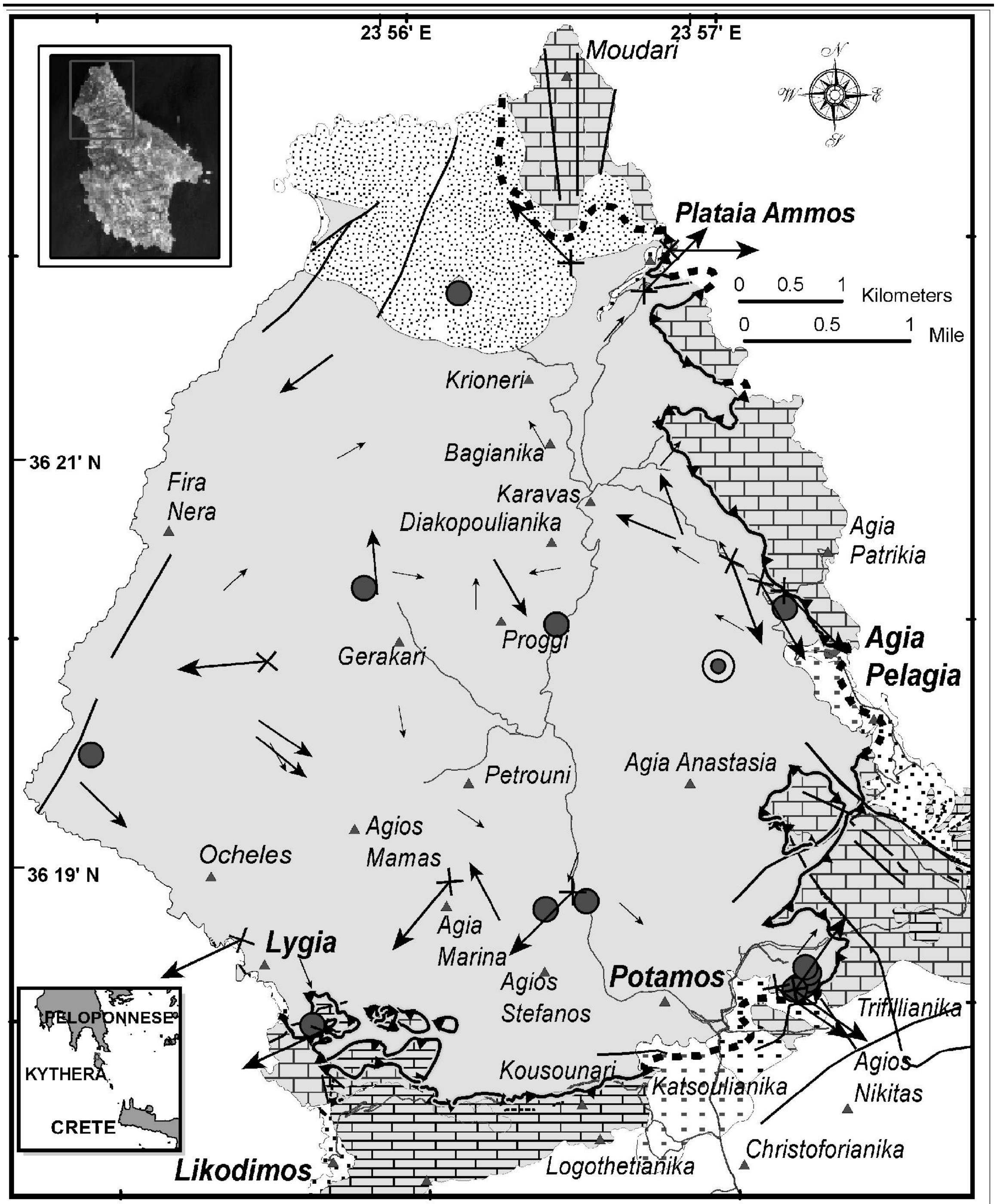

Figure 1a: Geological Map of North Kythera including the Potamos Detachment Fault (PDF), (Marsellos, 2006).

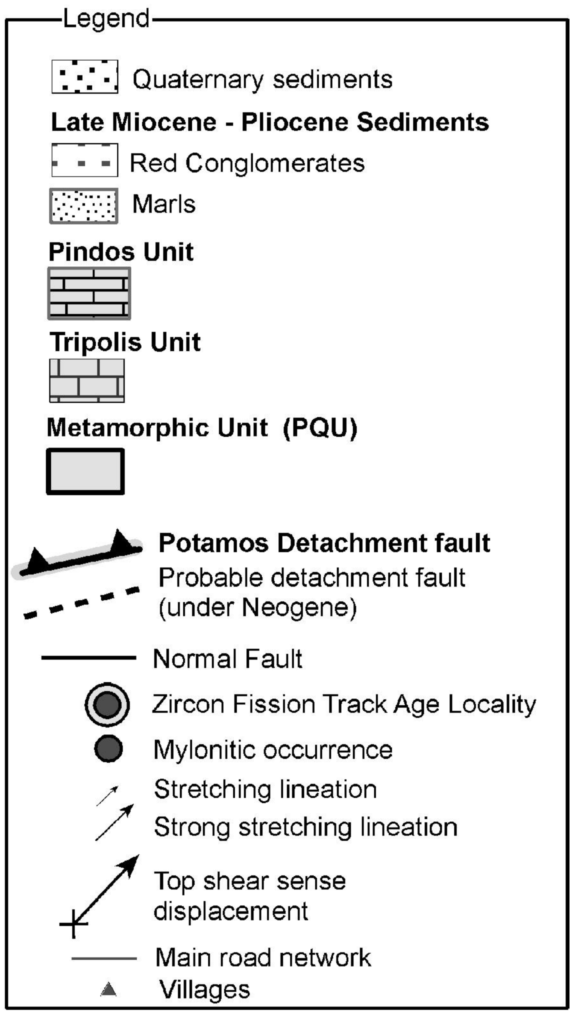

Figure 1b: Legend for the geological map of North Kythera (Fig. 1a), (Marsellos, 2006).

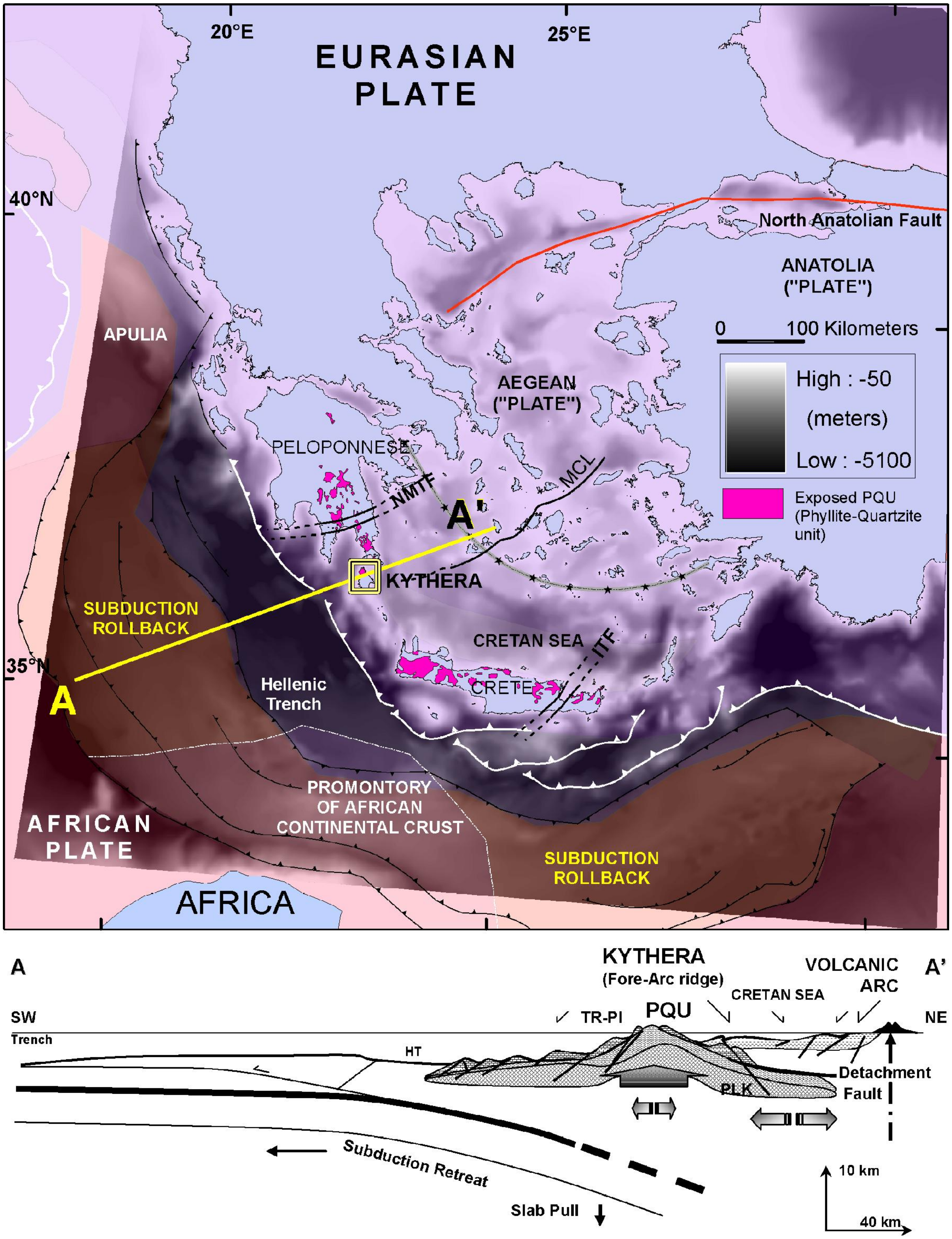

Figure 2: Tectonic setting of the South Aegean arc. Bathymetry shown by a semi-transparent DEM layer; a cross section line A - A' along a NE-SW line through the Kythera strait.

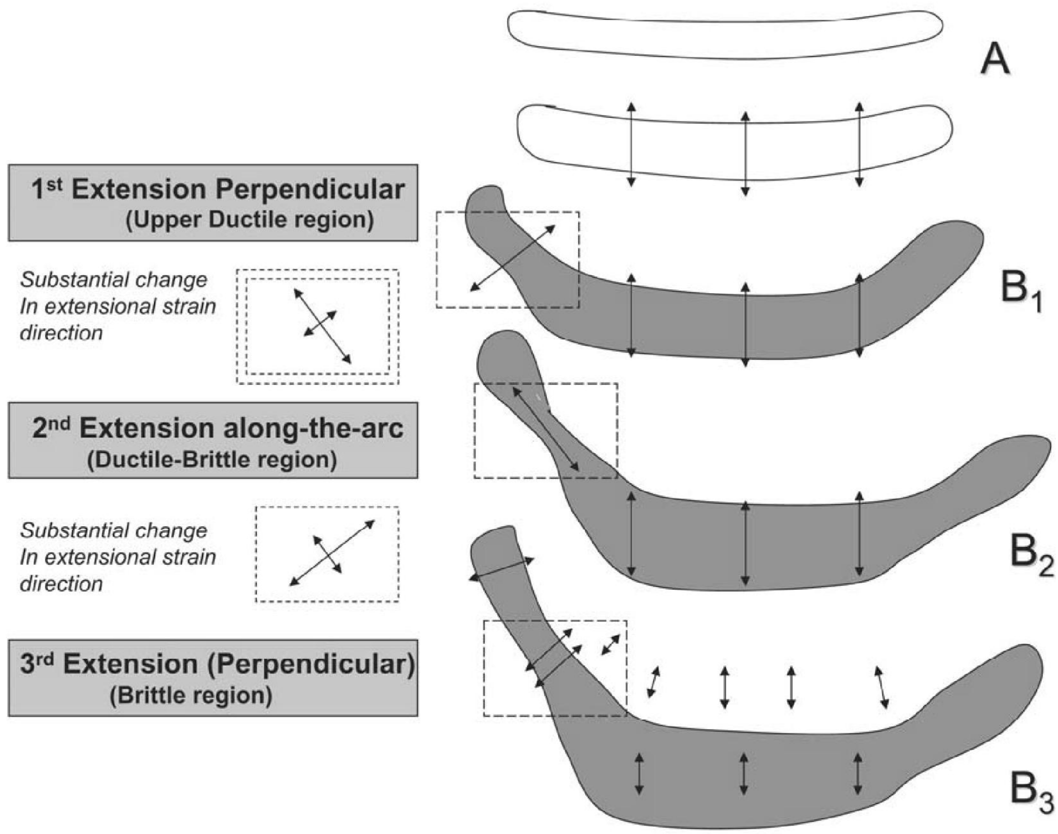

Figure 3: Extensional episodes of the southwest part of the Hellenic fore arc ridge (Marsellos, 2006b). Boxed area represents the region including Kythera.

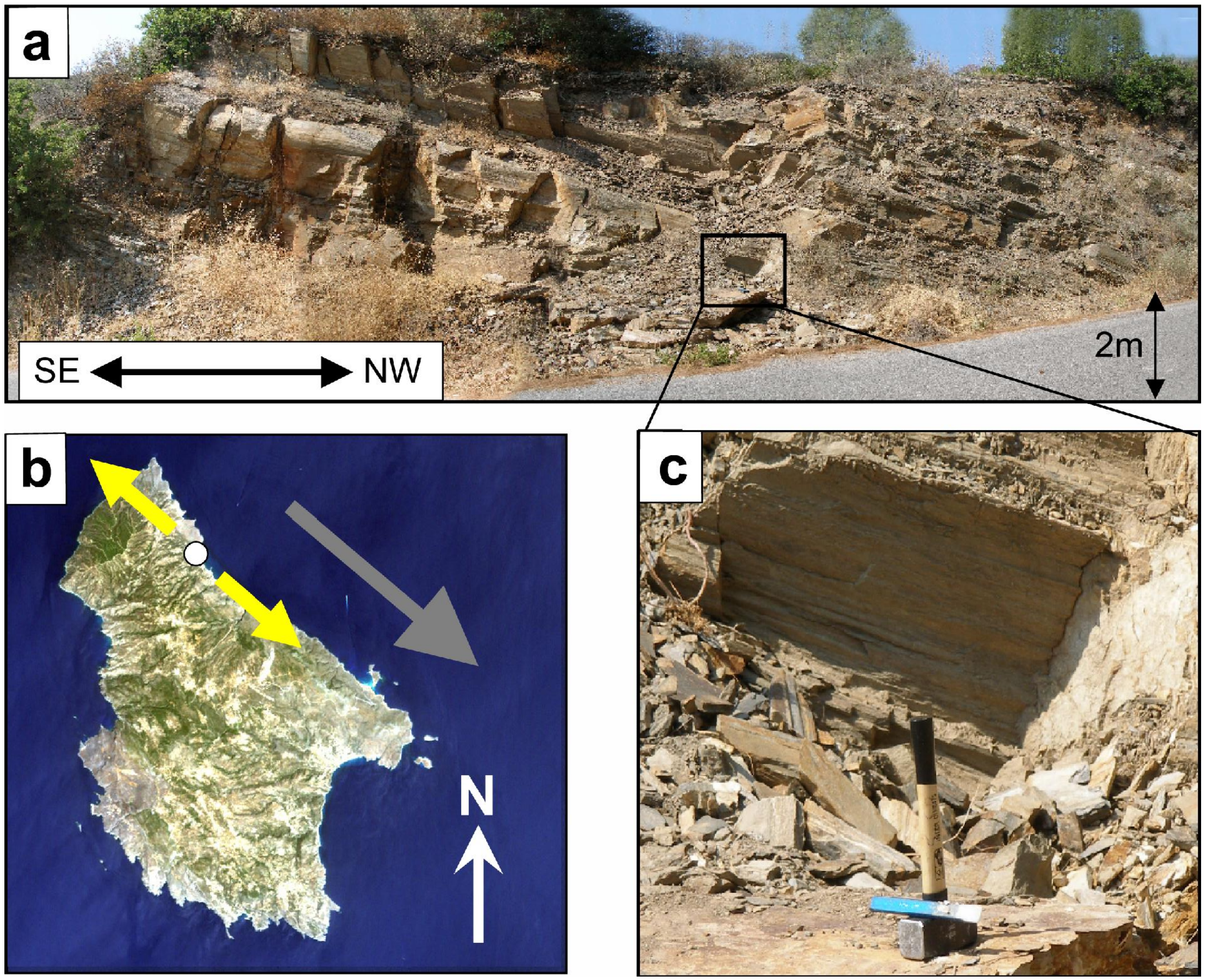

Figure 4: (a,c) Strong stretching lineation (the principal transport vector) plunging gently northwest, in outcrop close to Agia Pelagia area. b. Map shows outcrop location (white spot) and white arrows the direction of extension and the grey arrow the shear sense (top to SE).

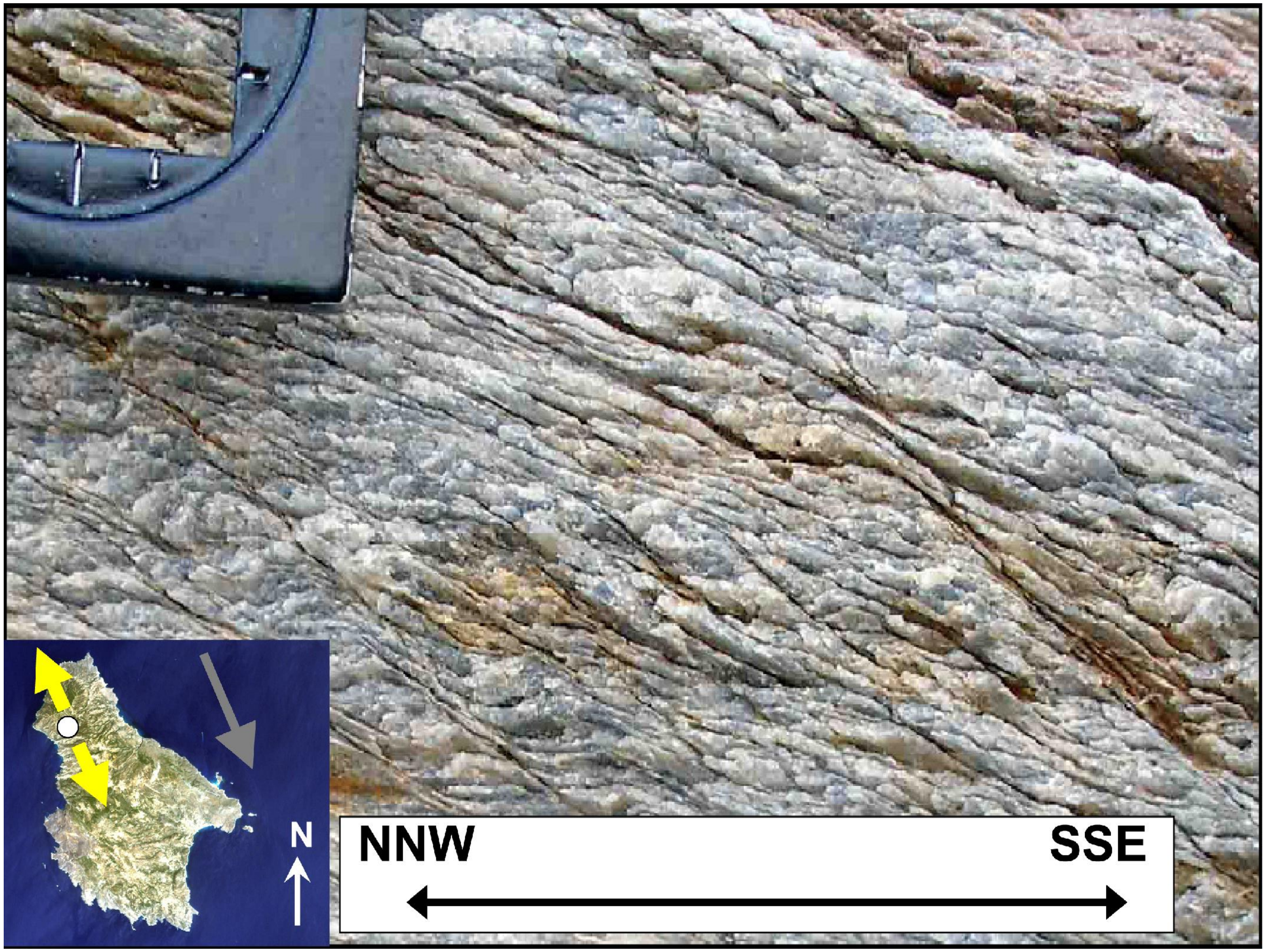

Figure 5: Vertical outcrop face showing asymmetric structure of an S/C fabric in an outcrop north of Potamos village. White spot in map inset shows the outcrop location, white arrows are the extension direction and the grey arrow the shear sense (top to SSE).

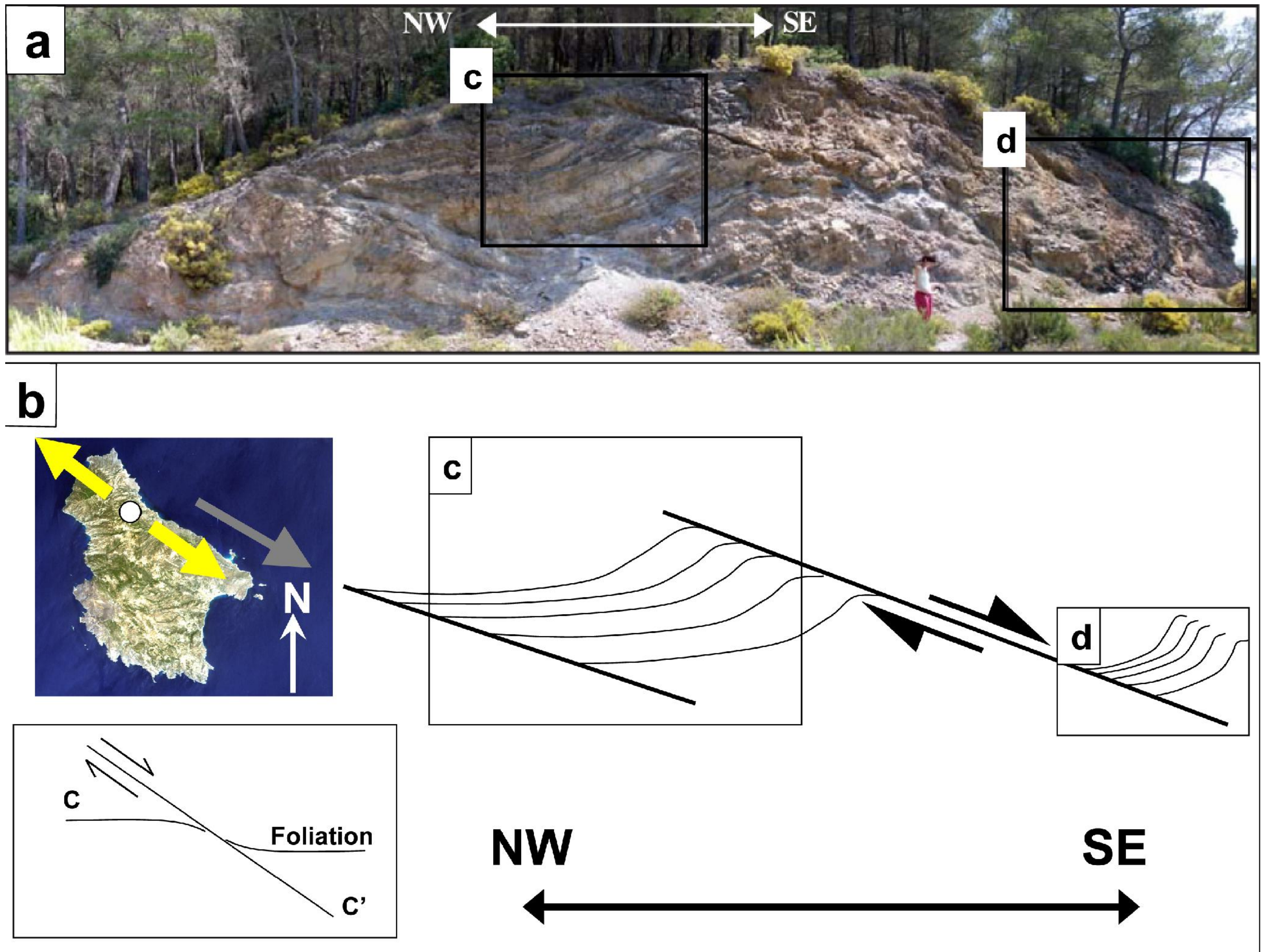

Figure 6: (a). Outcrop of a C/C' shear band fabric close to the detachment and mylonite, in the Potamos area. (b).Interpretation of this structure. On index map white spot shows the outcrop locality; white arrows show the extension direction; grey arrow indicates the shear sense (top to SE).

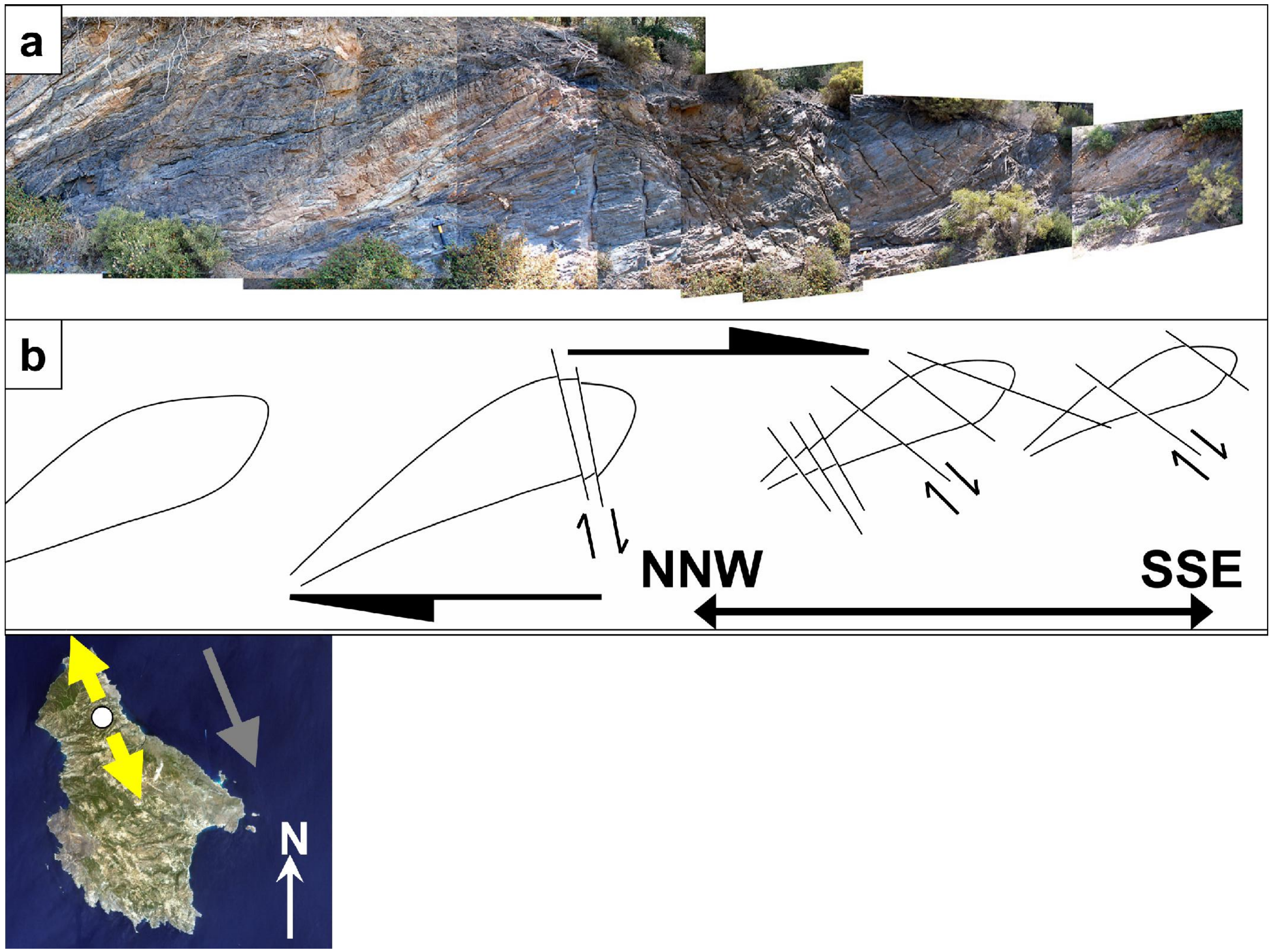

***Figure** 7*: Quartzite layers (lighter) in phyllite series (grey), showing boudinage from NNE-SSW trending-extension, close to Potamos mylonites. On index map, white spot shows outcrop location, white arrows are the extension direction and the grey arrow the sense of shear (top to SSE).

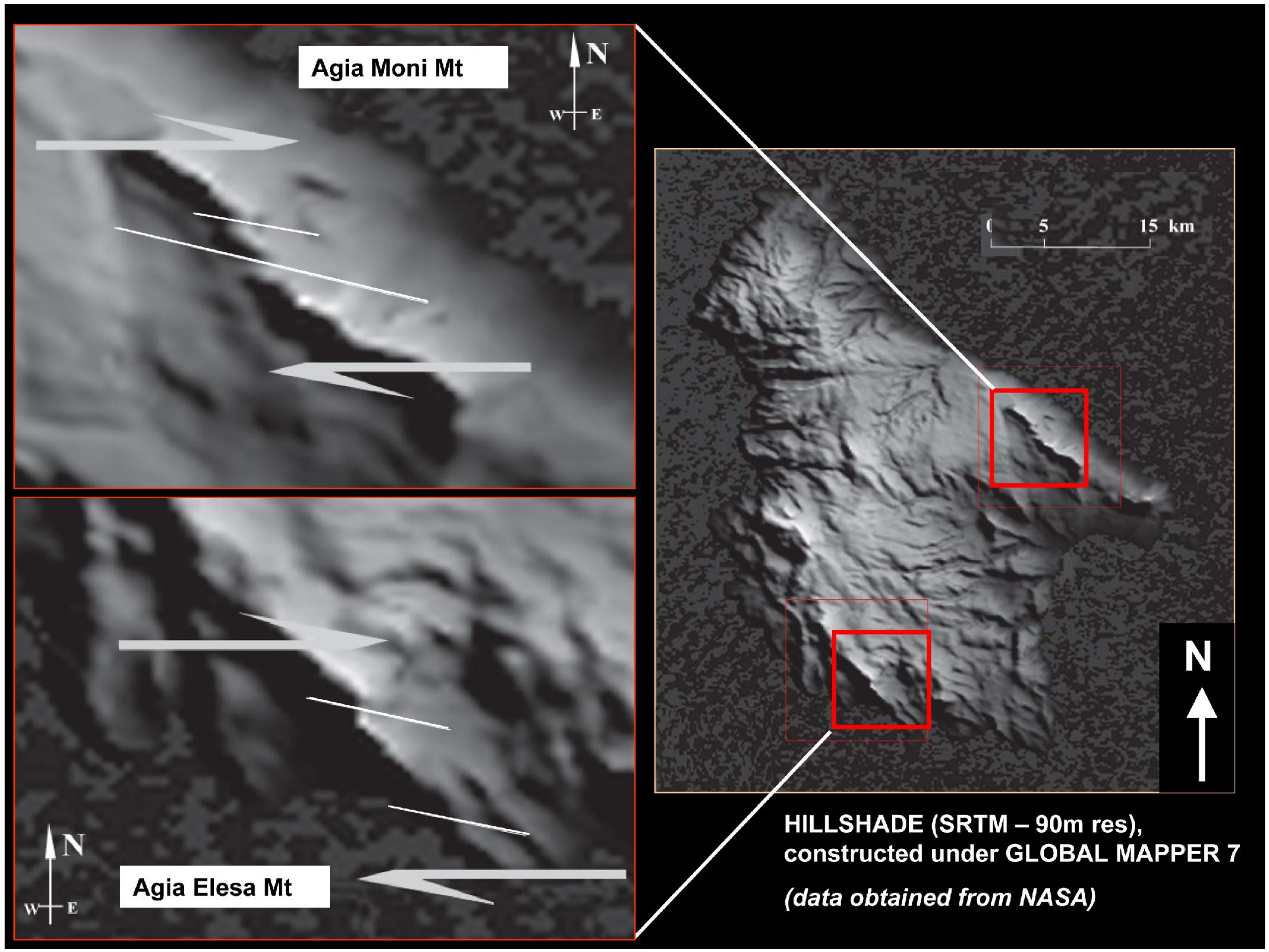

Figure 8: (right) A grayscale gradient Digital Elevation Model of Kythera constructed from SRTM (Shuttle Radar Terrain Model) of 3 arc-sec resolution. (left) Enlargment of parts of the DEM. Top left is Agia Moni area, and bottom left is Agia Elesa area. The ridgeline offsets suggest dextral slip sense on faults of near E-W strike; they may be Riedel fractures in a wider zone of shear.

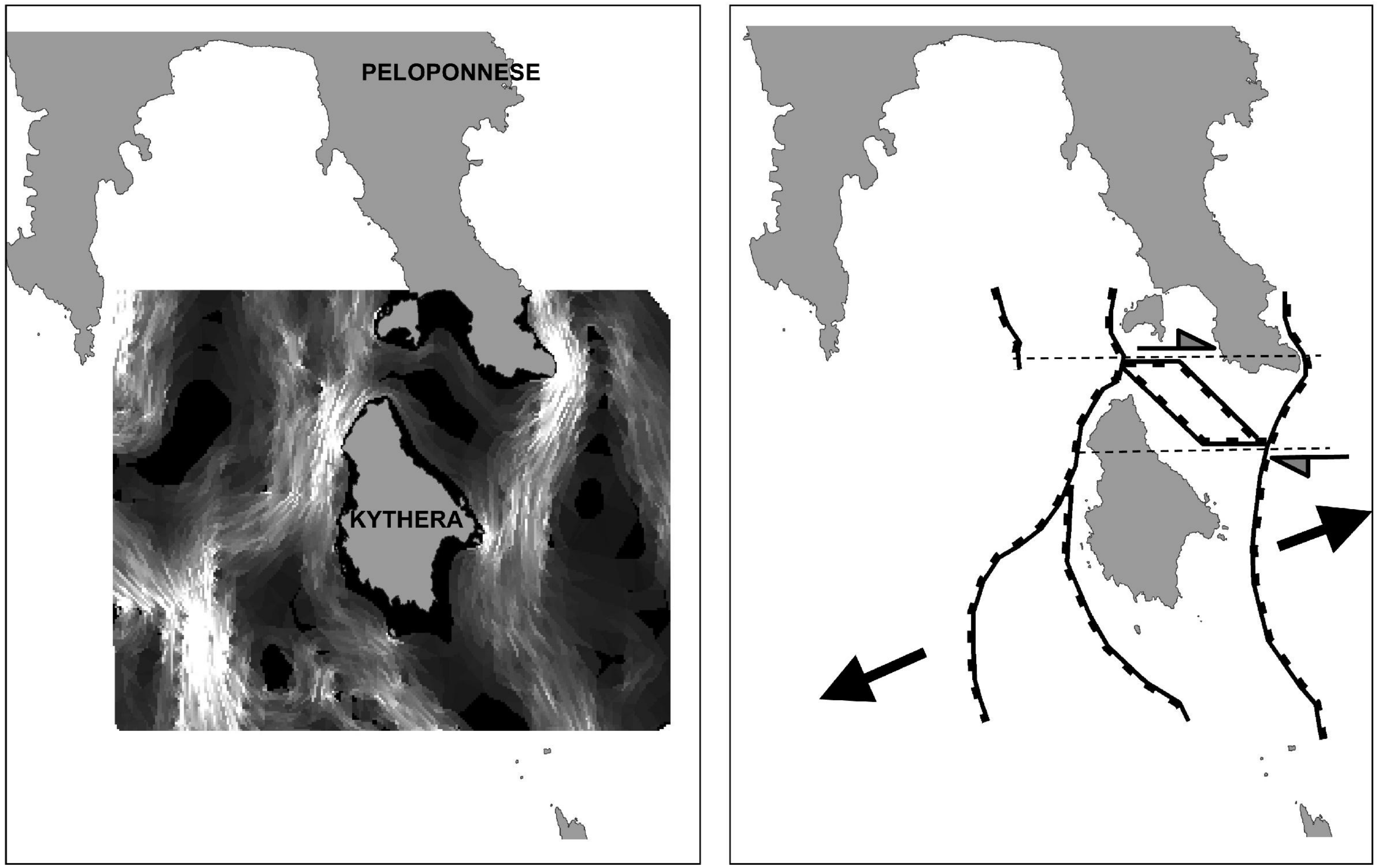

Figure 9: Interpretation of the present major submarine faults around Kythera. The background image is a submarine slope map in which probable submarine faults form areas of highest slope, shown white). These scarps show systematic dextral bending in a zone (the black dashed lines) running near the north end of Kythera, and a probable small dextral pull-apart basin between the Peloponnese and Kythera. Black arrows show orientation of inferred active extension perpendicular to dominant fault strike.

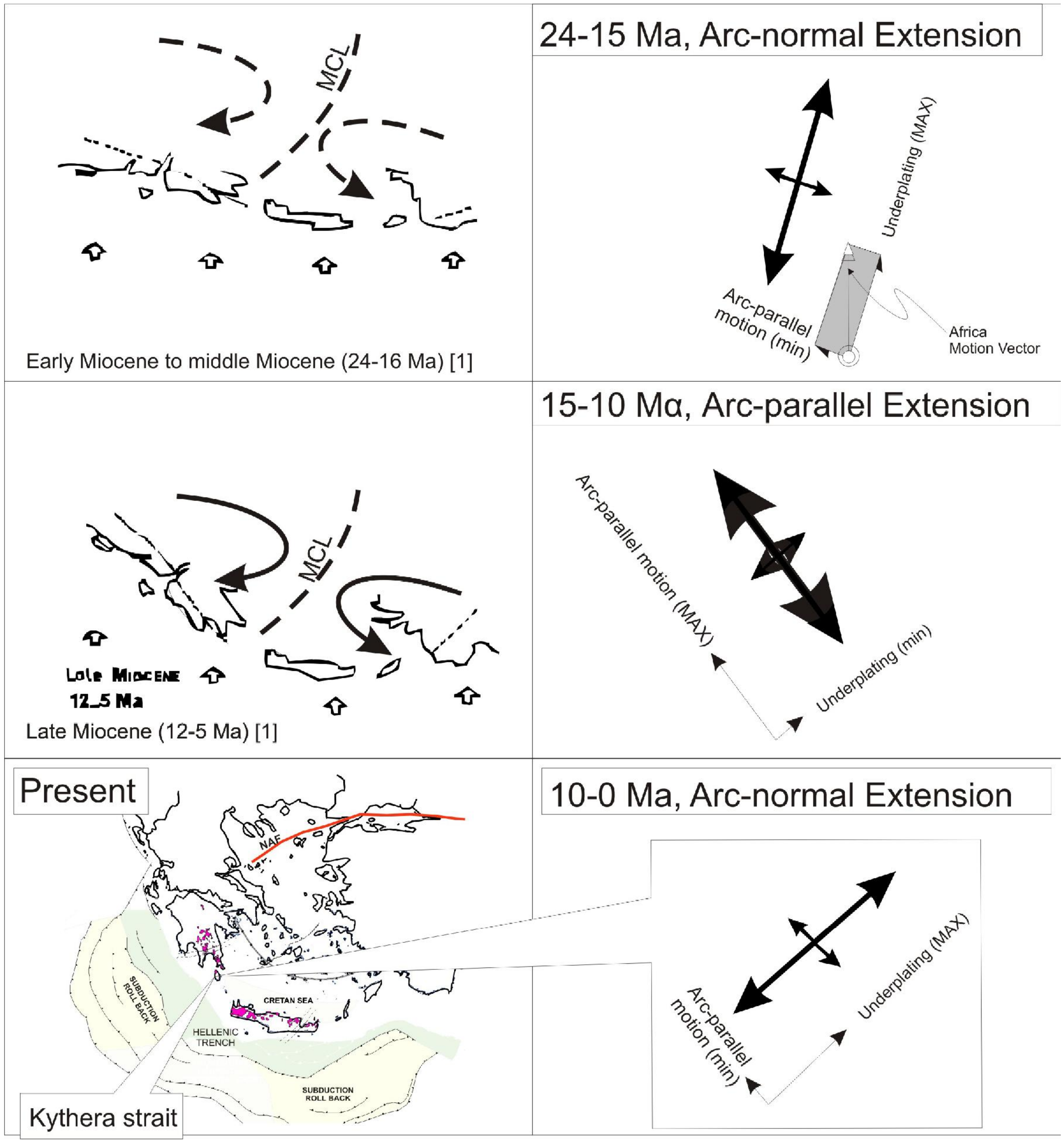

Figure 1a: Partitioning of the arc-normal (high decoupling-underplating activity) and arc-parallel component (low decoupling-underplating activity, prominent extension along-the-arc structures). Rotation figure boxes after [1] Kissel and Laj, (1988).

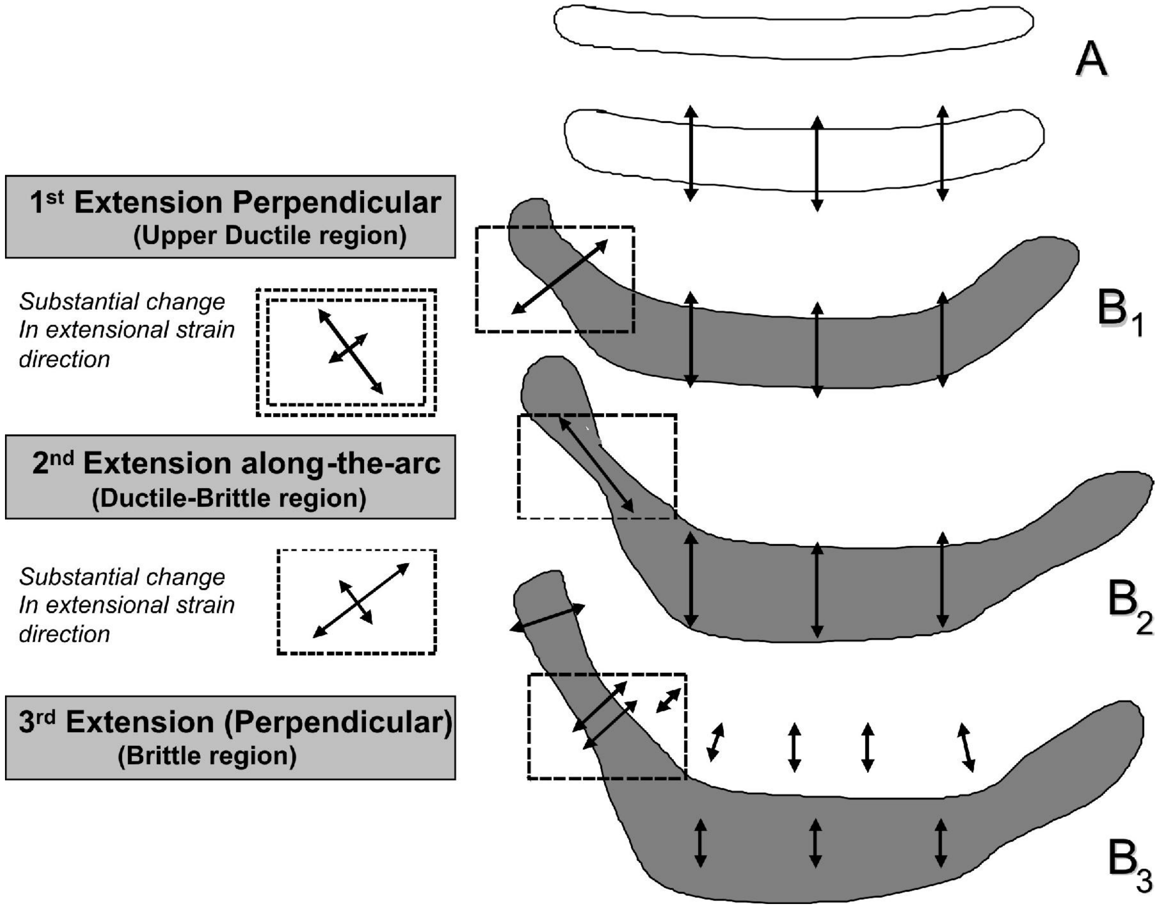

Figure 1b: Extensional episodes of the southwest part of the Hellenic fore arc ridge (Marsellos, 2006b). Boxed area represents the region including Kythera.

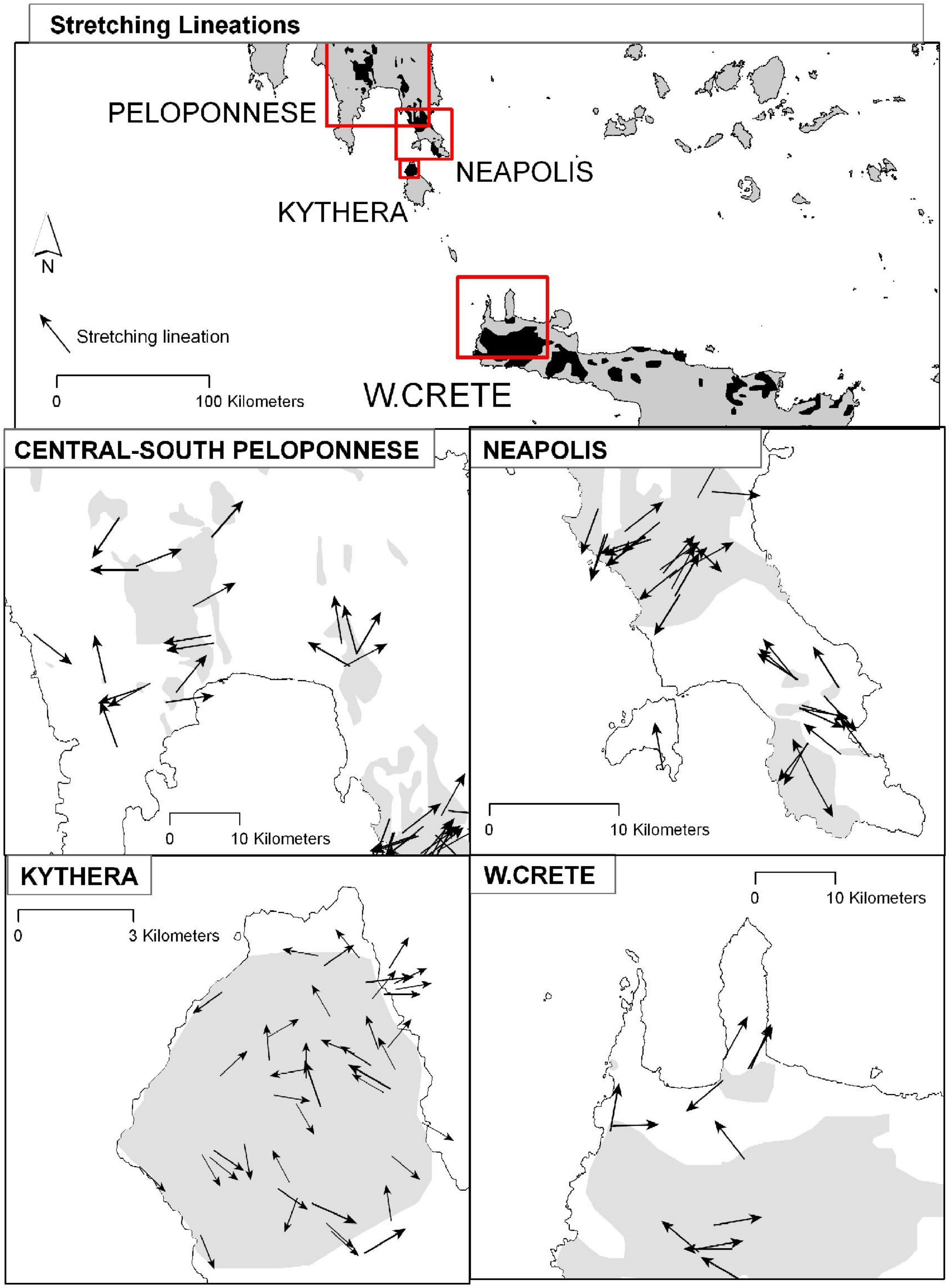

Figure 2: Distribution of stretching lineations in the PQU of Peloponnese, Kythera, and western Crete. a) Index map (PQU shown black). b) central-south Peloponnese; c) Neapolis, southeastern Pelopononese; d) nothern Kythera; e) western Crete; PQU outcrop areas shown by grey in detailed maps.

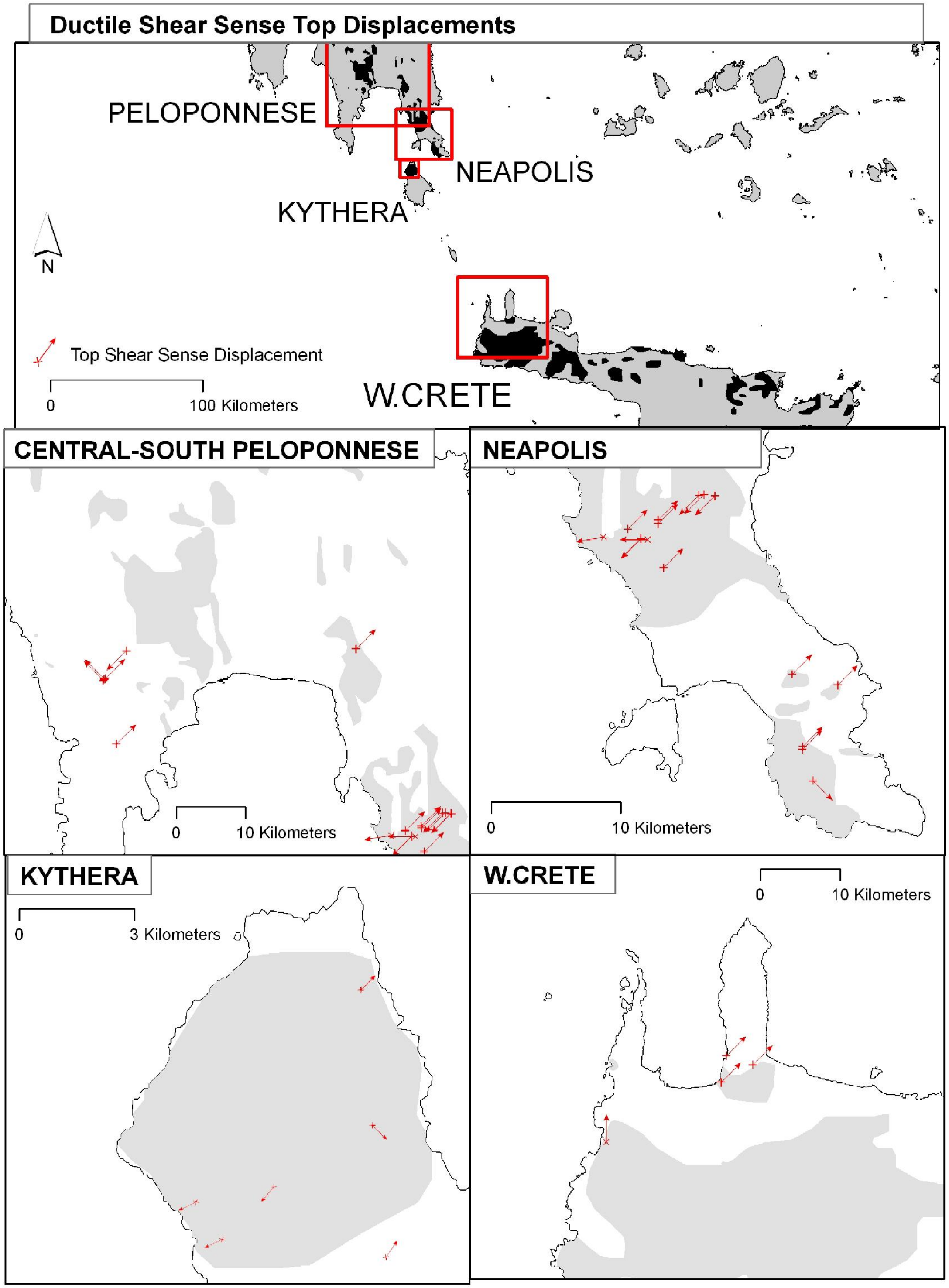

Figure 3: Distribution of ductile shear sense top displacement in the PQU of Peloponnese, Kythera, and western Crete. a) Index map (PQU shown black). b) central-south Peloponnese; c) Neapolis, southeastern Pelopononese; d) nothern Kythera; e) western Crete; PQU outcrop areas in detailed maps shown by grey.

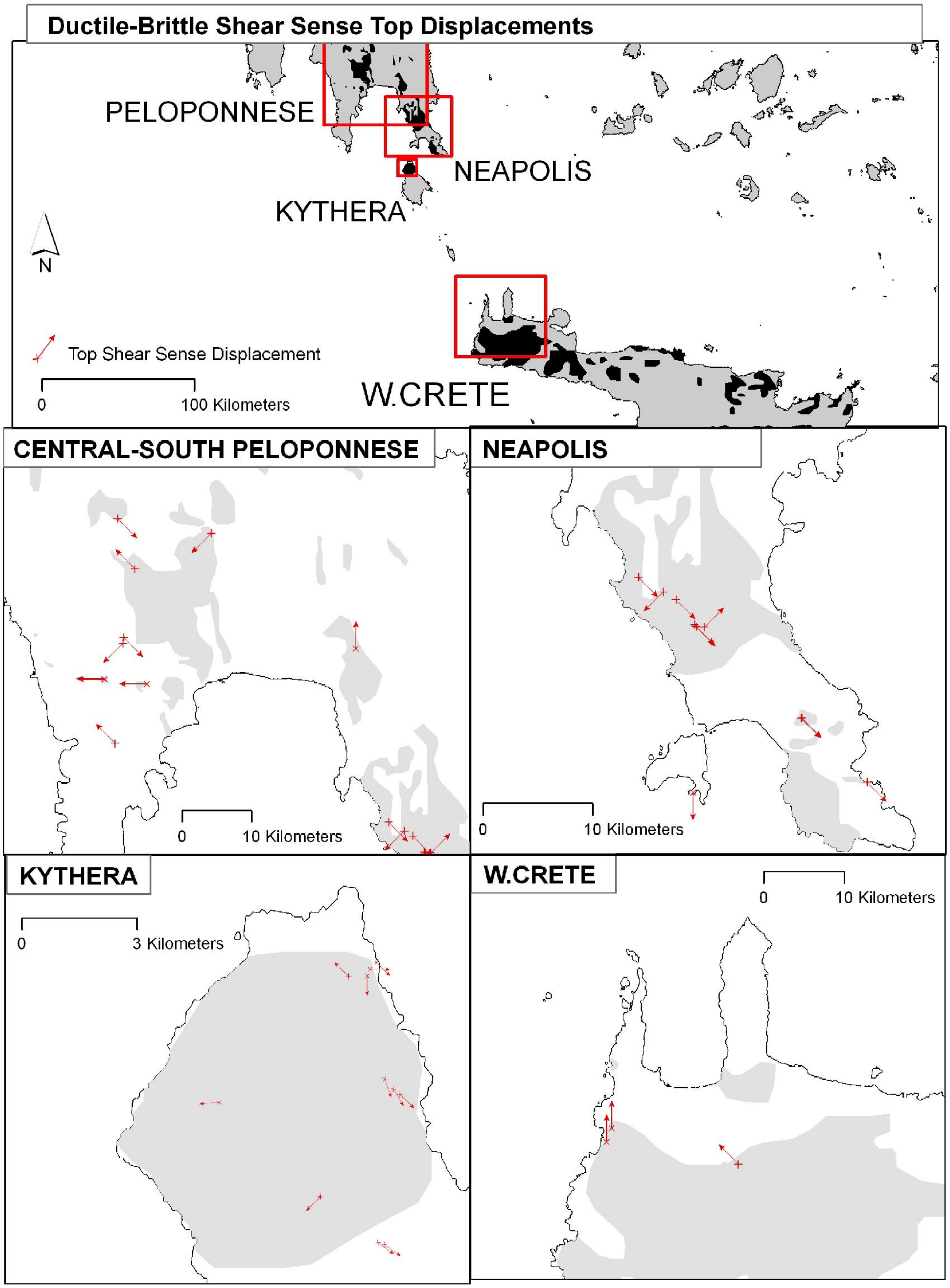

Figure 4: Distribution of ductile-brittle shear sense top displacement in the PQU of Peloponnese, Kythera, and western Crete. a) Index map (PQU shown black). b) central-south Peloponnese; c) Neapolis, southeastern Pelopononese; d) nothern Kythera; e) western Crete; PQU outcrop areas shown in detailed maps by grey.

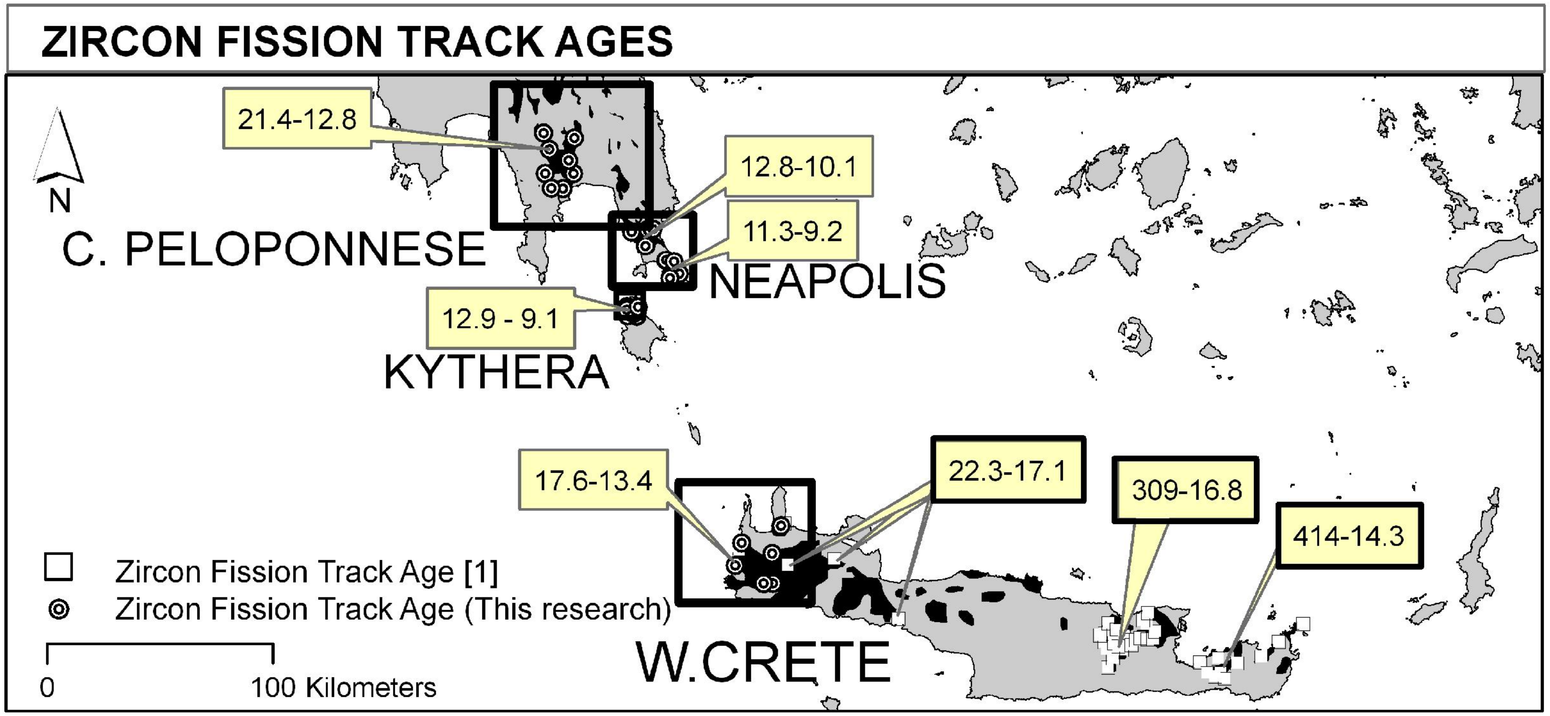

Figure 5a: Distribution of zircon fission track ages in the Phyllite-Quartzite Unit of Peloponnese, Kythera, and western Crete. Index map of the following (next page) b,c,d,e detailed maps. ZFT ages from this research whose sample localities are shown by circles, while ZFT age ranges in bold-outline boxes from eastern Crete and some from western Crete are from [1] Brix et al., (2002), and are shown by open squares in the index map. The black areas in the index map indicate the outcrops of the PQU.

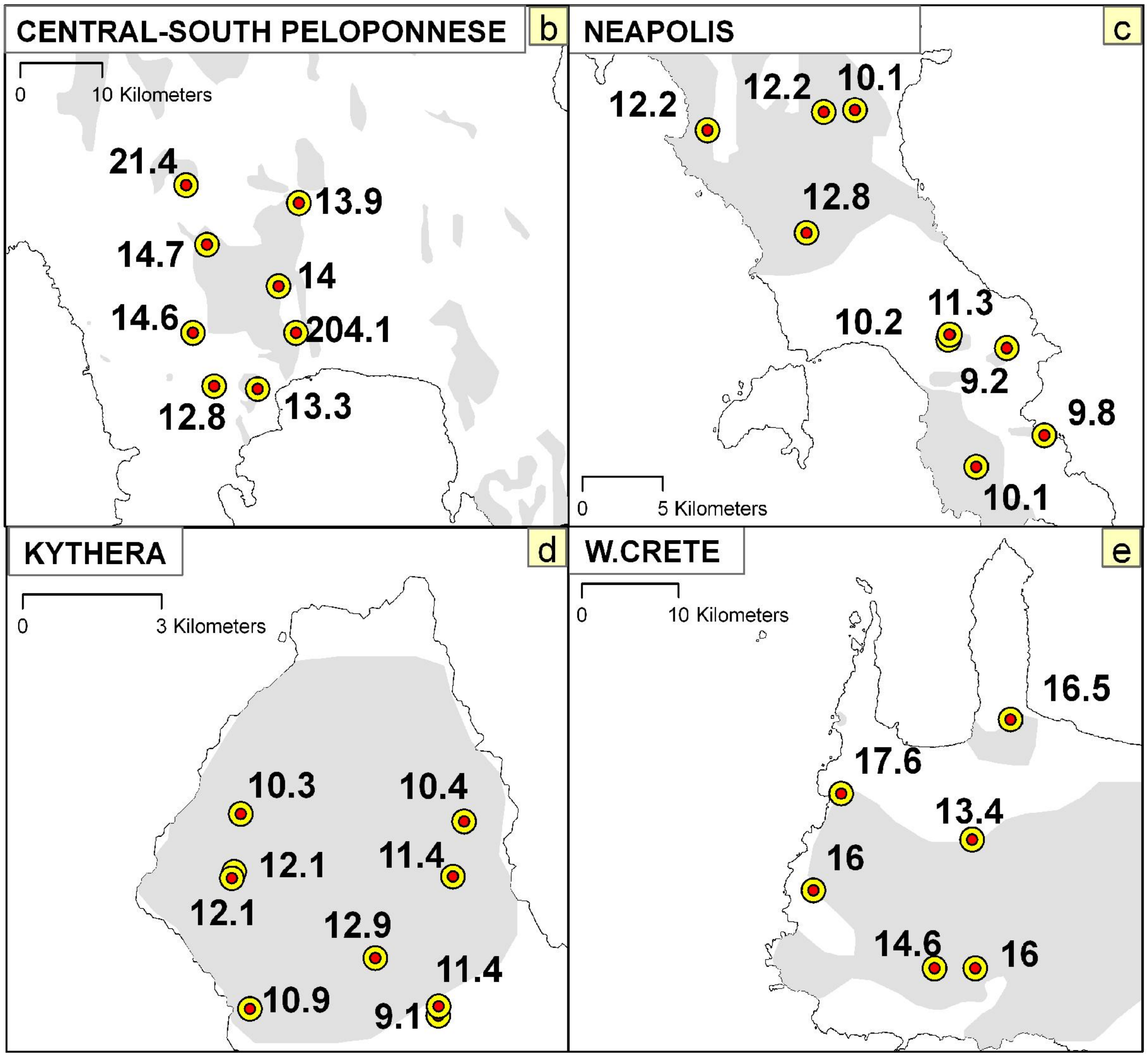

Figure 5 (b-e): Distribution of zircon fission track ages in the Phyllite-Quartzite Unit of Peloponnese, Kythera, and western Crete. ZFT ages from this research are shown by circles; b) central Peloponnese; c) southern Pelopononese; d) nothern Kythera; e) western Crete; PQU outcrop areas shown by grey.

Table 1: Summary of zircon fission-track data from the Hellenic Forearc ridge.

			ZETA Age program													Binomfit Program	
Sample	Elev	Mineral	ρs	Ns	ρi	Ni	ρd	Nd	n	χ^2	Age	-1σ	+1σ	U+/-2se	Age Dispersion (%)	*Primary Age (Ma)*	*Secondary Age (Ma)*
Peloponnese																	
AAP4	348	Zircon	1.12E+07	123	4.29E+07	471	2803	2.349E+05	15	3.7%	14.6	-3	+6.2	146.4 ±14.2	33.8	*14.6*	*5.7*
PAA-1	487	Zircon	1.08E+07	79	4.79E+07	407	2801	2.358E+05	3	16.7%	8.8	-1	+1.2	937.4 ±97.1	2.5	*8.7*	
PAA-2	480	Zircon	1.96E+07	207	8.08E+07	851	2798	2.375E+05	15	1.3%	14.7	-1.1	+1.3	275.7 ±20.5	28.8	*14.7*	*8.1*
D01	109	Zircon	1.91E+07	183	7.75E+07	737	2765	2.571E+05	15	37.1%	12.2	-1	+1.1	228.2 ±18	8.3	*11.3*	*20.9*
D03	222	Zircon	2.50E+07	264	9.68E+07	1020	2762	2.588E+05	15	8.9%	12.8	-0.9	+1	303.3 ±20.8	17.3	*11.0*	*16.2*
D08	365	Zircon	1.98E+07	210	8.20E+07	857	2759	2.605E+05	15	20.4%	12.2	-1	+1.1	252.1 ±18.6	11.7	*12.2*	
D09	223	Zircon	1.61E+07	177	7.97E+07	868	2756	2.622E+05	15	48.9%	10.2	-0.9	+0.9	237 ±17.5	1.2	*10.2*	
D10	288	Zircon	1.82E+07	192	8.11E+07	856	2753	2.639E+05	15	40.9%	11.3	0.9	+1	249.6 ±18.6	12.6	*12.4*	*8.6*
D13	151	Zircon	5.81E+07	622	6.75E+07	741	2750	2.656E+05	24	0.0%	9.2	-2.6	+2.8	131.7 ±10.4	94.4	*9.2*	*84.4*
D18	15	Zircon	1.73E+07	182	9.01E+07	951	2747	2.673E+05	15	88.7%	9.8	-0.8	+0.9	277.2 ±19.9	0.2	*9.8*	
D20	75	Zircon	2.56E+07	266	1.34E+08	1358	2744	2.690E+05	28	61.9%	10.1	-0.7	+0.8	209.2 ±13.1	1.8	*10.1*	
D24	112	Zircon	1.33E+07	146	6.93E+07	747	2741	2.707E+05	14	15.7%	10.1	-0.9	+1	218.7 ±17.4	15.1	*9.3*	*16.0*
D25	48	Zircon	2.14E+07	226	8.38E+07	883	2738	2.724E+05	15	65.0%	13.3	-1	+1.1	249.4 ±18.6	26.3	*13.3*	
D26	157	Zircon	2.02E+07	224	8.20E+07	919	2735	2.741E+05	15	61.3%	12.8	-1	+1.1	243.8 ±18	4.7	*12.8*	
D28	153	Zircon	1.66E+08	1477	4.21E+07	375	2733	2.758E+05	15	0.0%	204.1	-13	+13.9	119 ±12.9	56.4	*215.4*	*39.4*
D29	270	Zircon	1.69E+07	178	6.42E+07	677	2730	2.775E+05	15	55.0%	14	-1.2	+1.3	187.7 ±15.8	0.3	*14.0*	
D30	105	Zircon	1.73E+07	*157*	6.44E+07	*602*	2727	2.792E+05	15	57.5%	13.9	-1.3	+1.4	187.8 ±16.7	1.1	*13.9*	
D32	677	Zircon	2.96E+07	289	7.33E+07	726	2724	2.809E+05	15	36.3%	21.4	-1.6	+1.7	211.2 ±17.4	8.9	*21.3*	
Kythera																	
D43	77	Zircon	2.97E+07	310	1.55E+08	1614	2720	2.826E+05	28	87.0%	10.4	-0.7	+0.8	241.2 ±14.9	0.4	*10.4*	
T04	123	Zircon	2.43E+07	304	5.36E+07	696	1938	1.303E+05	18	81.7%	10.9	-0.8	+0.9	259 ±21.6	0.2	*10.9*	
T06	341	Zircon	2.70E+07	291	7.15E+07	787	1922	1.292E+05	15	94.9%	9.1	-0.7	+0.8	475.7 ±37.9	0.1	*9.1*	
T07	345	Zircon	2.61E+07	307	5.66E+07	662	1906	1.281E+05	15	47.2%	11.4	-0.8	+0.9	366.8 ±31.5	0.4	*11.4*	
T13	366	Zircon	1.83E+07	223	3.34E+07	420	1890	1.270E+05	15	45.8%	12.9	-1.1	+1.2	214.3 ±22.4	9.7	*12.9*	
T14	298	Zircon	1.87E+07	191	4.17E+07	437	1850	1.243E+05	15	40.9%	10.4	-0.9	+1	274.6 ±28.6	14.8	*10.4*	
T15	353	Zircon	1.37E+07	152	2.69E+07	295	1834	1.232E+05	15	45.1%	12.1	-1.2	+1.4	178.1 ±22.1	12.9	*12.1*	
T18	298	Zircon	1.84E+07	230	3.53E+07	443	1818	1.222E+05	17	84.1%	12.1	-1	+1.1	206.3 ±21.6	0.9	*12.1*	
QZ12	155	Zircon	1.68E+07	160	6.16E+07	580	2313	2.167E+05	20	81.8%	11.4	-1	+1.1	176.5 ±16.1	0.2	*11.4*	
Crete																	
CR01	51	Zircon	1.71E+07	172	4.64E+07	481	2792	2.409E+05	15	24.5%	16.5	-1.5	+1.6	148.7 ±14.2	12.7	*18*	*10.3*
CR07	246	Zircon	2.26E+07	278	5.92E+07	733	2788	2.434E+05	15	72.4%	17.6	-1.3	+1.4	186.6 ±14.7	0.7	*17.1*	
CR09	521	Zircon	6.33E+07	756	1.78E+08	2064	2785	2.443E+05	36	16.7%	16	-0.8	+0.9	241.8 ±12.6	15.6	*15.7*	*21.3*
CR11	561	Zircon	6.30E+07	649	2.01E+08	2076	2776	2.494E+05	35	0.3%	13.4	-1.1	+1.3	276 ±14.2	24.2	*12.5*	*20.2*
CR14	867	Zircon	9.96E+07	1126	2.99E+08	3394	2772	2.519E+05	44	28.3%	16.1	-0.7	+0.8	313.9 ±13.8	9.9	*15.1*	*21.7*
CR15	305	Zircon	3.12E+07	341	1.05E+08	1135	2768	2.545E+05	21	25.2%	14.6	-1	+1.1	250.4 ±16.4	17.6	*12.5*	*19.6*

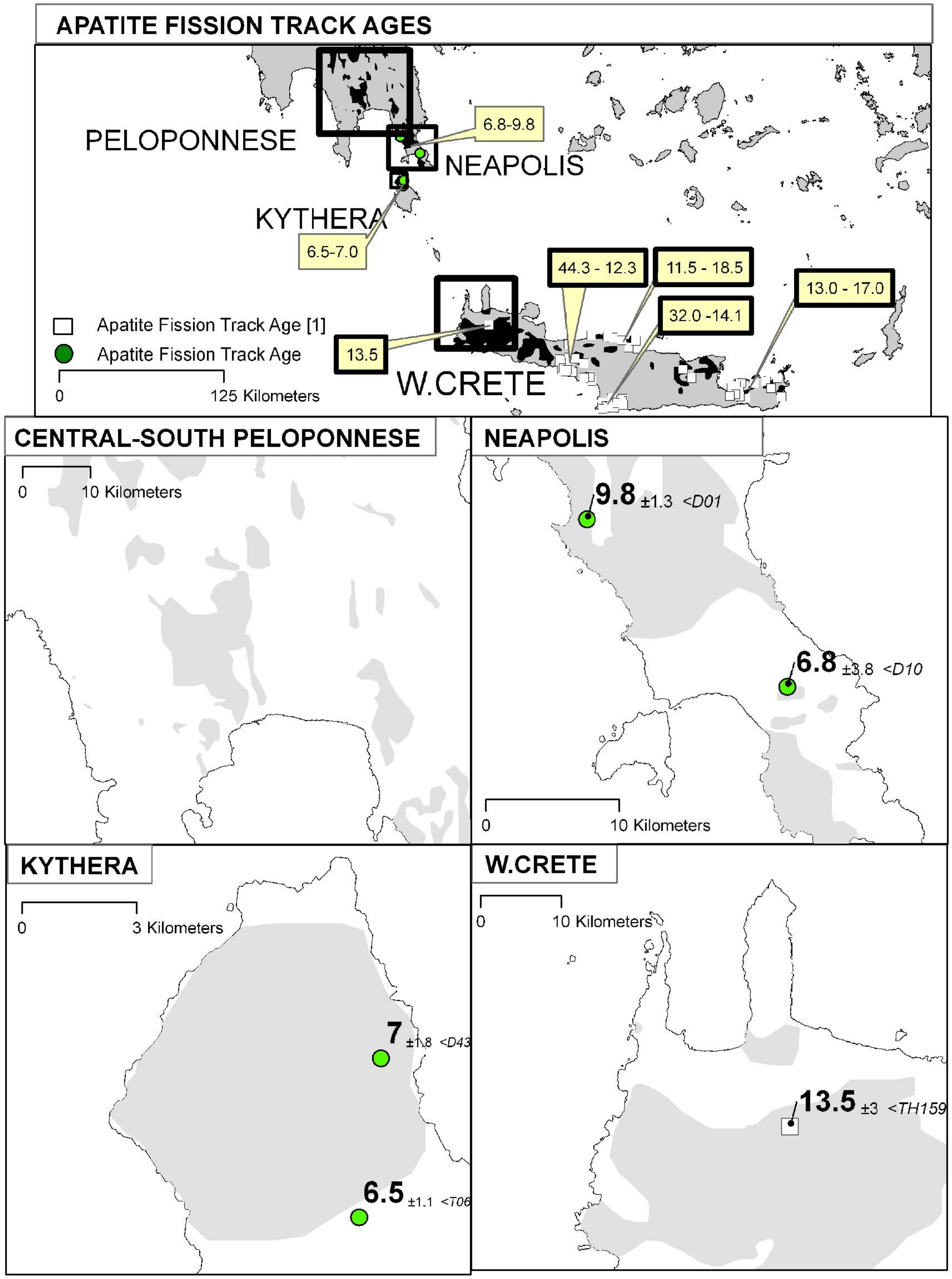

Figure 6: Distribution of apatite fission track ages in the Phyllite-Quartzite Unit of Peloponnese, Kythera, and western Crete. a) Index map. The black areas indicate the outcrops of the PQU; b) central Peloponnese; c) southern Pelopononese; d) nothern Kythera; e) western Crete. The AFT ranges shown with bold outline boxes, and age (square) shown in Crete are from [1] Thomson et al. (1998).

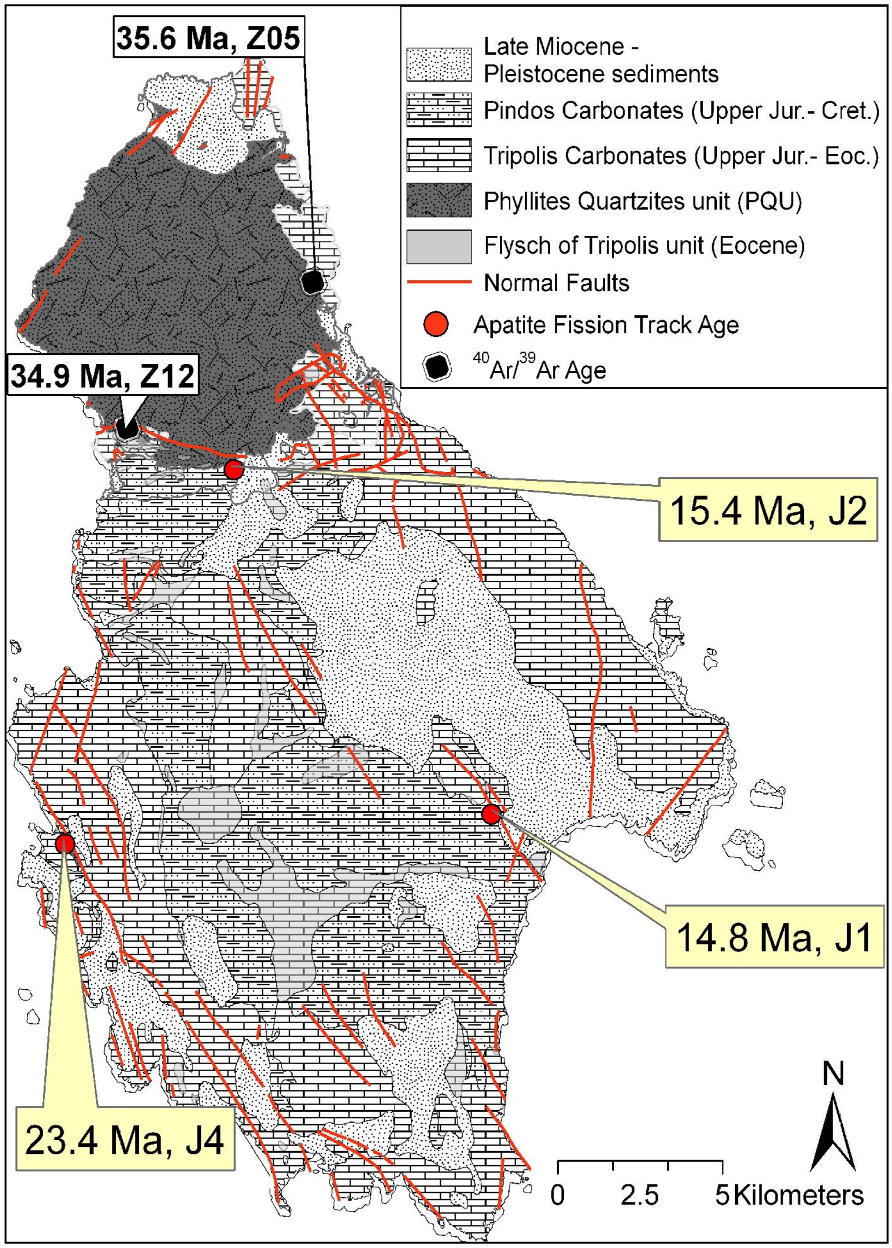

Figure 7 : Sample locations of AFT ages from upper plate (Tripolis flysch), and $^{40}Ar/^{39}Ar$ ages on Kythera Island. Simplified geological map of Kythera, after Petrocheilos et al. (1966) and our observations.

Table 2: Summary of apatite fission-track data from the Hellenic Fore-Arc ridge.

Sample	Elev	Mineral	ρs	Ns	ρi	Ni	ρd	Nd	n	χ^2	Age	-1σ	+1σ	U+/-2se
Peloponnese														
D01	109	Apatite	**2.28E+06**	77	**3.81E+07**	1341	2689	3.513E+06	16	38.3%	9.8	-1.2	+1.4	24.9 ±1.5
D10	288	Apatite	**7.34E+04**	5	**2.42E+06**	133	2718	3.652E+06	27	69.1%	6.8	-3.1	+4.4	0.7 ±0.1
Kythera (Upper Plate)														
J1	89	Apatite	6.00E+05	15	6.07E+06	152	2597	3.085E+06	7	71.7%	14.8	-4.0	+5.0	11.7 ±1.9
J2	314	Apatite	1.70E+06	43	1.44E+07	370	2603	3.111E+06	9	66.7%	15.4	-2.7	+3.0	20.6 ±2.3
J4	61	Apatite	2.22E+06	106	1.69E+07	690	2614	3.161E+06	15	0.0%	23.4	-2.6	+3.0	14.7 ±1.2
Kythera (Lower Plate)														
D43	77	Apatite	**7.76E+05**	20	**1.58E+07**	486	2684	3.488E+06	9	64.3%	7.0	-1.6	+1.9	22.5 ±2.1
T06	341	Apatite	**2.65E+06**	48	**6.20E+07**	1187	2649	3.325E+06	14	78.2%	6.5	-1.0	+1.1	44.1 ±2.9

Note: Elevations are given in meters, ρs is the density (cm^2) of spontaneous tracks and Ns is the number of spontaneous tracks counted; ρi is the density (cm^2) of induced tracks; and ρd is the density (cm^2) of tracks on the fluence monitor (CN5); n is the number of grains counted; and χ^2 is the Chi-squared probability (%). Fission track ages (± 1σ) were determined using the Zeta method, and ages were calculated using the computer program and equations in Brandon (1992). All ages with $\chi^2 > 5\%$ are reported as pooled ages. A Zeta factor for zircon of 382.20 ±11.00 (± 1 se) is based on 11 determinations from both the Fish Canyon Tuff and the Buluk tuff. Glass monitors (CN5 for zircon), placed at the top and bottom of the irradiation package were used to determine the fluence gradient. All samples were counted at 1250x using a dry 100x objective (10x oculars and 1.25x tube factor) on an Olympus BMAX 60 microscope fitted with an automated stage and a digitizing tablet.

Table 3: $^{40}Ar/^{39}Ar$ analytical data.

	ID	Temp (°C)	$^{40}Ar/^{39}Ar$	$^{37}Ar/^{39}Ar$	$^{36}Ar/^{39}Ar$ (x 10^{-3})	$^{39}Ar_K$ (x 10^{-15} mol)	K/Ca	$^{40}Ar^*$ (%)	^{39}Ar (%)	Age (Ma)	±1s (Ma)
	T 11, Biotite, 9.8 mg, J=0.0013823±1.09%, D=1.004±0.001, NM-207D, Lab#=57071-01										
x	A	640	1753.8	0.5190	706.9	0.240	0.98	88.1	9.8	2062.2	12.7
x	B	665	517.2	0.2695	227.0	0.068	1.9	87.0	12.5	872.9	16.0
x	C	715	499.4	0.1123	118.9	0.084	4.5	93.0	16.0	894.5	14.2
x	D	765	1870.2	0.0861	369.5	0.099	5.9	94.2	20.0	2226.0	21.0
x	E	840	775.2	0.1650	176.8	0.383	3.1	93.3	35.6	1250.1	9.8
x	F	910	31.44	0.0180	29.64	0.591	28.3	72.1	59.7	**55.7**	1.2
x	G	990	34.53	0.0658	26.66	0.543	7.8	77.2	81.9	65.3	1.5
x	H	1065	42.67	0.1937	42.35	0.325	2.6	70.7	95.1	73.7	1.9
x	I	1140	148.2	1.053	338.4	0.051	0.48	32.7	97.2	117.1	13.3
x	J	1240	153.4	5.749	353.3	0.031	0.089	32.3	98.4	119.9	19.7
x	K	1640	457.2	2.391	1237.3	0.038	0.21	20.1	100.0	215.9	24.4
	Integrated age ± 1s			n=11		2.45	1.9	K2O=0.07%		764.7	7.1
	Plateau ± 1s	no plateau		n=0	MSWD=0.00	0.000			0.0	0.00	0.000
	Z05, Biotite, 7.7 mg, J=0.0013838±1.08%, D=1.004±0.001, NM-207D, Lab#=57072-01										
x	A	640	192.4	0.3764	282.7	0.259	1.4	56.6	11.8	253.2	4.3
x	B	665	45.75	0.2906	19.72	0.081	1.8	87.3	15.5	97.1	8.5
x	C	715	72.79	0.0817	29.18	0.108	6.2	88.2	20.5	153.5	8.6
x	D	765	321.0	0.1367	106.0	0.114	3.7	90.3	25.7	608.3	10.4
x	E	840	249.8	0.1894	119.1	0.292	2.7	85.9	39.0	469.2	4.6
	F	910	15.67	0.1151	8.305	0.508	4.4	84.4	62.2	**32.7**	1.6
	G	990	16.99	0.3357	8.612	0.455	1.5	85.2	83.0	**35.8**	1.9
	H	1065	22.83	0.8834	13.78	0.223	0.58	82.5	93.1	**46.5**	3.2
x	I	1140	80.34	1.298	195.4	0.061	0.39	28.4	95.9	56.2	13.2
x	J	1240	70.77	1.668	118.0	0.045	0.31	50.9	98.0	87.9	16.6
x	K	1640	375.1	3.331	819.9	0.044	0.15	35.5	100.0	305.7	18.6
	Integrated age ± 1s			n=11		2.19	1.2	K2O=0.08%		174.3	2.3
	Plateau ± 1s	steps F-H		n=3	MSWD=7.19	1.19			54.1	**35.6**	**3.1**
	Z 12, Biotite, 8.3 mg, J=0.0013882±1.08%, D=1.004±0.001, NM-207D, Lab#=57073-03										
x	A	640	718.0	0.6058	757.1	0.107	0.84	68.8	5.0	942.9	14.4
x	B	665	140.2	0.1777	26.82	0.023	2.9	94.4	6.0	304.2	26.3
x	C	715	167.4	0.0093	105.4	0.051	55.0	81.4	8.4	312.5	11.1
x	D	765	358.8	0.1249	190.2	0.071	4.1	84.3	11.7	632.7	11.1
x	E	840	186.8	0.1466	106.1	0.225	3.5	83.2	22.1	352.6	3.7
	F	910	18.41	0.0357	15.00	0.614	14.3	75.9	50.6	**34.67**	0.97
	G	990	19.47	0.1555	15.56	0.442	3.3	76.5	71.0	**36.9**	1.3
	H	1065	21.49	0.1981	31.13	0.337	2.6	57.3	86.6	**30.6**	1.9
	I	1140	40.10	0.4771	81.21	0.155	1.1	40.4	93.8	40.1	4.6
	J	1240	59.09	1.034	134.1	0.061	0.49	33.1	96.6	48.3	10.0
x	K	1640	144.0	1.442	380.2	0.073	0.35	22.0	100.0	77.9	11.6
	Integrated age ± 1s			n=11		2.16	2.2	K2O=0.07%		160.7	2.1
	Plateau ± 1s	steps F-J		n=5	MSWD=2.69	1.61			74.5	**34.9**	**1.2**

***Table 3**:* $^{40}Ar/^{39}Ar$ analytical data (continue from previous page).

Notes:

Isotopic ratios corrected for blank, radioactive decay, and mass discrimination, not corrected for interfering reactions.
Errors quoted for individual analyses include analytical error only, without interfering reaction or J uncertainties.
Integrated age calculated by summing isotopic measurements of all steps.
Integrated age error calculated by quadratically combining errors of isotopic measurements of all steps.
Plateau age is inverse-variance-weighted mean of selected steps.
Plateau age error is inverse-variance-weighted mean error (Taylor, 1982) times root MSWD where MSWD>1.
Plateau error is weighted error of Taylor (1982).
Decay constants and isotopic abundances after Steiger and Jäger (1977).
symbol preceding sample ID denotes analyses excluded from plateau age calculations.
Weight percent K_2O calculated from ^{39}Ar signal, sample weight, and instrument sensitivity.
Ages calculated relative to FC-2 Fish Canyon Tuff sanidine interlaboratory standard at 28.02 Ma
Decay Constant (LambdaK (total)) = 5.543e-10/a
Correction factors:

$(^{39}Ar/^{37}Ar)_{Ca}$ = 0.0007 ± 5e-05
$(^{36}Ar/^{37}Ar)_{Ca}$ = 0.00028 ± 2e-05
$(^{38}Ar/^{39}Ar)_{K}$ = 0.0129
$(^{40}Ar/^{39}Ar)_{K}$ = 0 ± 0.002

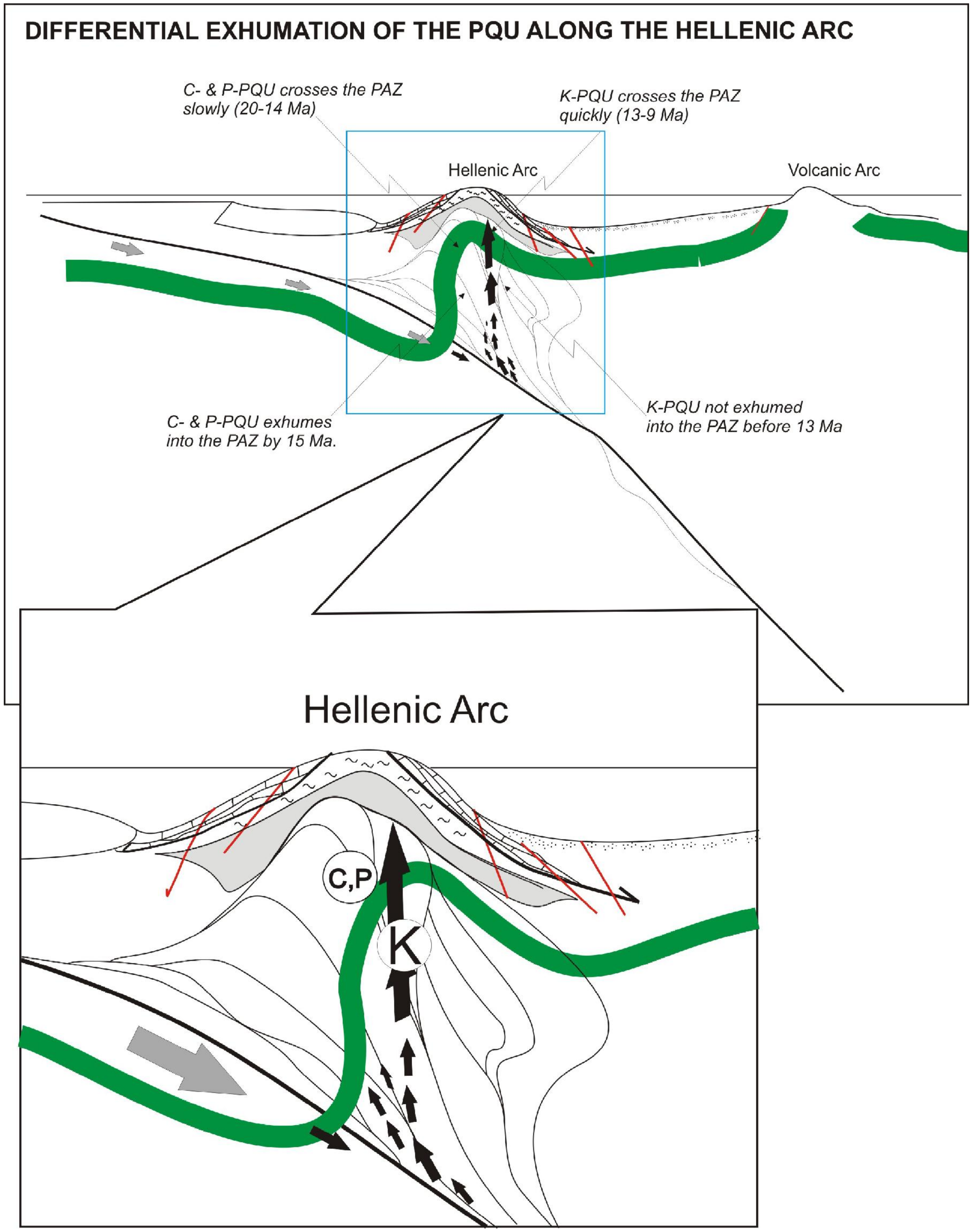

Figure 8: Kythera and southeastern Peloponnese PQU rocks (K) were situated at a lower crustal level after the first (arc-normal extension) stage compared to rocks of central Peloponnese PQU and Crete PQU (C,P) which reached the zircon FT PAZ. Localized along-arc stretching caused Kythera and Southeastern Peloponnese rocks to exhume quickly through the zircon FT PAZ between 13-9 Ma.

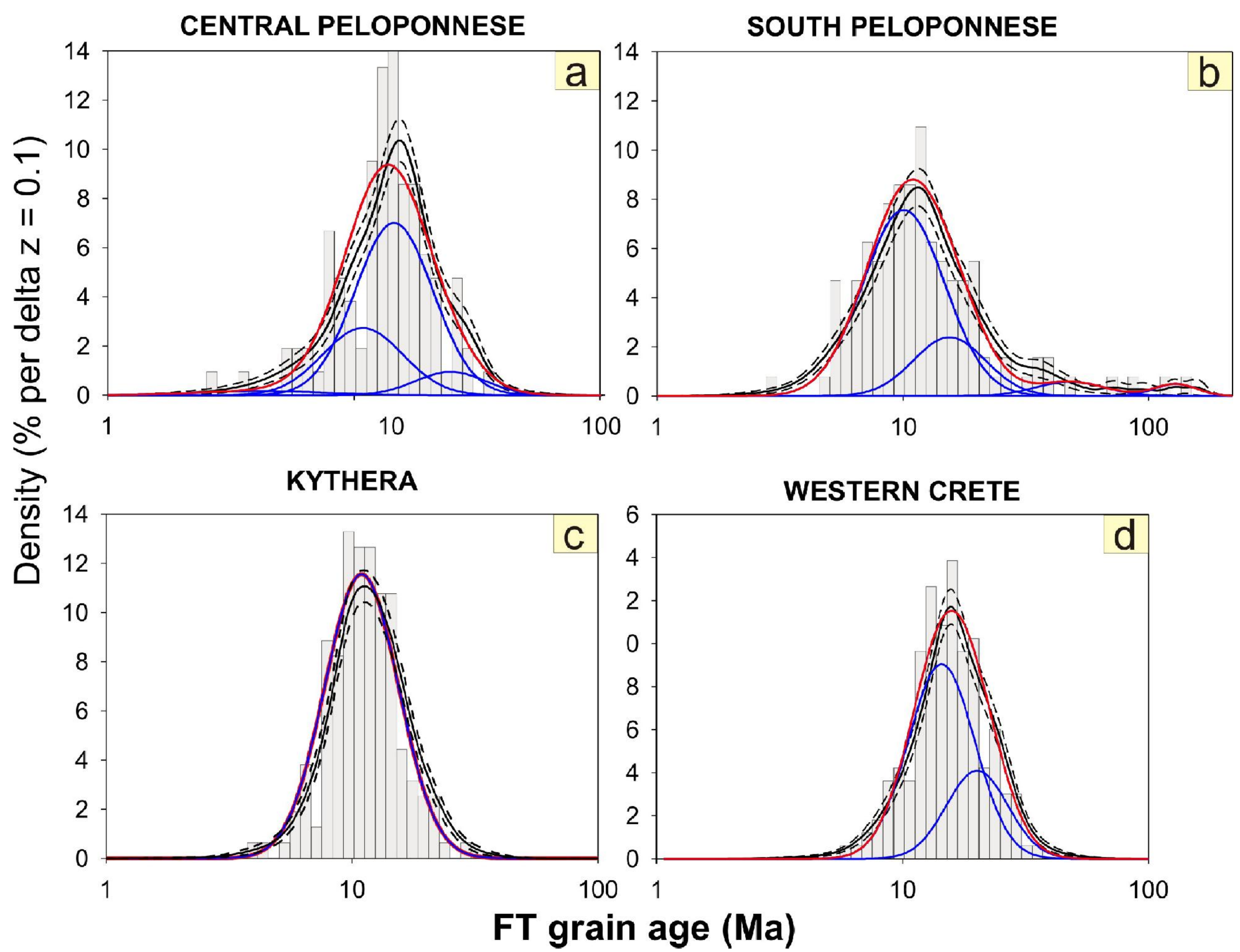

Figure 9: Results from binomial peak-fitting (Brandon, 1996) represented through the probability density plots. On these plots, the observed distribution is reported together with the individual histogram peaks representing the grain-age components. Black solid lines represent the observed grain-age distribution and grey areas represent the individual peaks. ZFT grain ages are from the exposed PQU rocks (lower plate): a) seven samples from the PQU of central Peloponnese. b) nine samples from the PQU of southern Peloponnese. c) nine samples from the PQU of Kythera. d) six samples from PQU of western Crete.

Table 4: Summary of Zircon Fission Track first and second peak ages using Binomfit program (Brandon, 1996).

	First Peak				Second Peak				
All Samples from	Peak (Ma)	68% CI		Frac. %	Peak (Ma)	68% CI		Frac. %	grains
S. & C. Peloponnese	**10.0**	-0.8	+0.8	51.0%	**14.1**	-1.3	+1.4	42.3%	276
South Peloponnese only	**10.1**	-0.7	+0.7	72.7%	**15.5**	-2.9	+3.5	20.2%	121
Central Peloponnese only	**14.6**	-1.5	+1.6	64.1%	**10.9**	-1.9	+2.3	25.6%	105
Kythera	**10.9**	-0.4	+0.5	100.0%					157
W.Crete	**14.4**	-0.8	+0.8	70.5%	**20.1**	-1.9	+2.2	29.5%	163

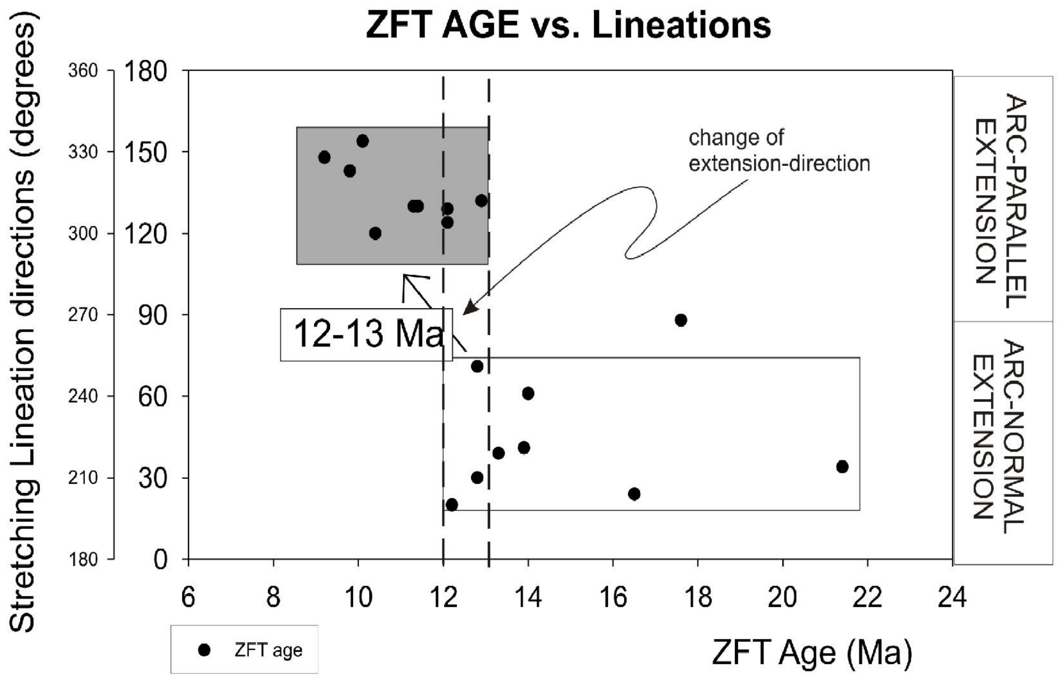

Figure 10: Observed orientation of the stretching lineations of the exposed PQU rocks is plotted together with the individual zircon fission track ages. The grey shaded box contains the ZFT ages of PQU rocks having a strong arc-parallel extensional stretching lineation.

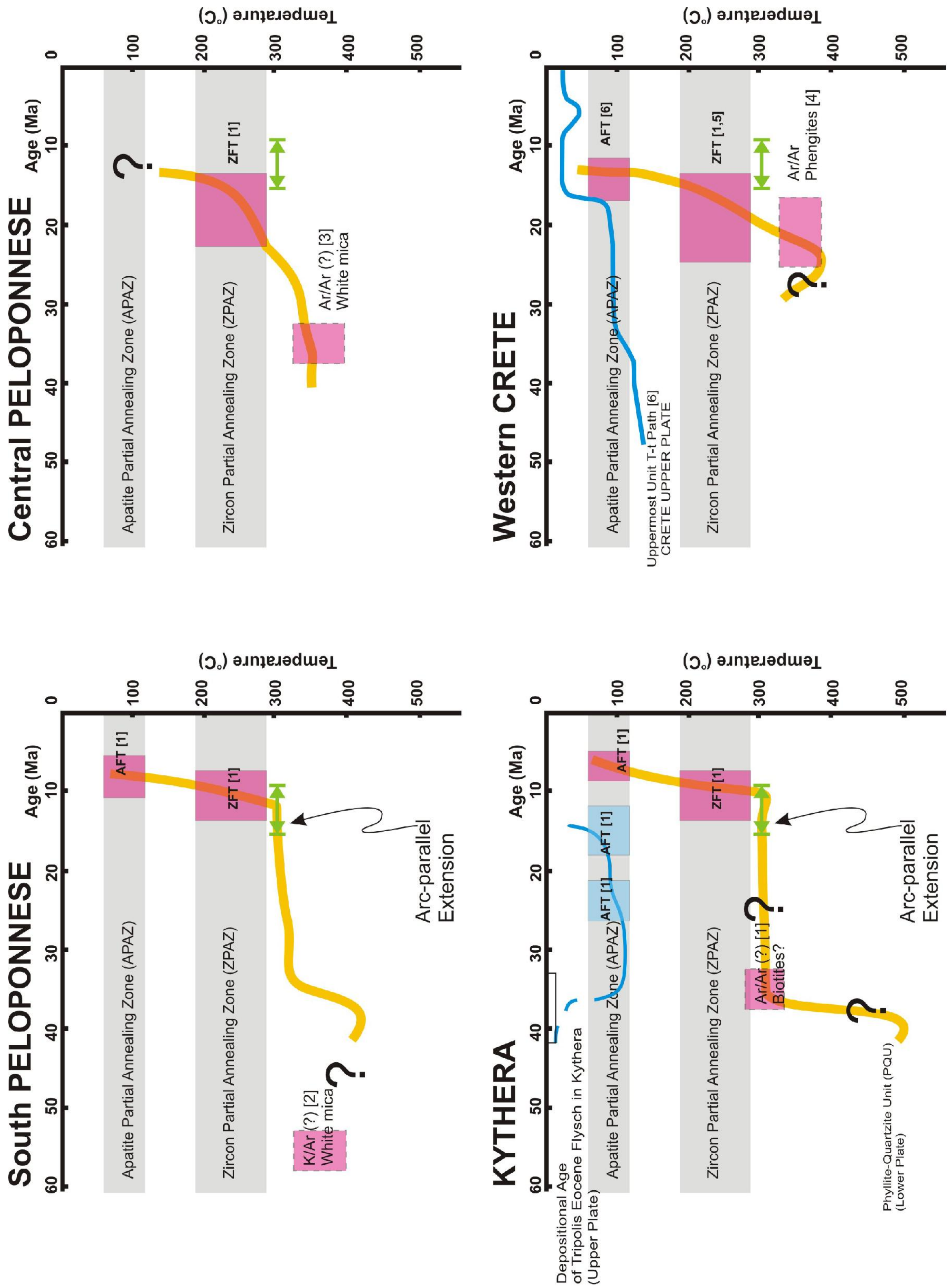

South PELOPONNESE
Central PELOPONNESE
KYTHERA
Western CRETE
Age (Ma)
Temperature (°C)
Apatite Partial Annealing Zone (APAZ)
Zircon Partial Annealing Zone (ZPAZ)
AFT [1]
ZFT [1]
K/Ar (?) [2]
White mica
Ar/Ar (?) [3]
White mica
Arc-parallel
Extension
AFT [6]
ZFT [1,5]
Ar/Ar
Phengites [4]
Uppermost Unit T-t Path [6]
CRETE UPPER PLATE
Ar/Ar (?) [1]
Biotites?
Depositional Age
of Tripolis Eocene Flysch in Kythera
(Upper Plate)
Phyllite-Quartzite Unit (PQU)
(Lower Plate)

Figure 11 *(previous page)*: Temperature-time (T-t) diagram for selected parts of the western Hellenic Arc combining: [1] apatite and zircon fission-track data and Ar-Ar data of this study, [2] K-Ar data of Seidel et al. (1982); [3] Ar-Ar data of Panagos et al. (1979), [4] Ar-Ar data of Jolivet et al. (1996), [5] ZFT data of Brix et al. (2002), and [6] AFT data of Thomson et al. (1997). T-t history of Uppermost unit of Crete derived by Thomson et al. (1998). T-t history of central and south Peloponnese, Kythera and westernmost Crete from this research. Reddish boxes and orange line are PQU metamorphics of "lower plate" of detachment; blue boxes and line are sandstones of "upper plate" of detachment.

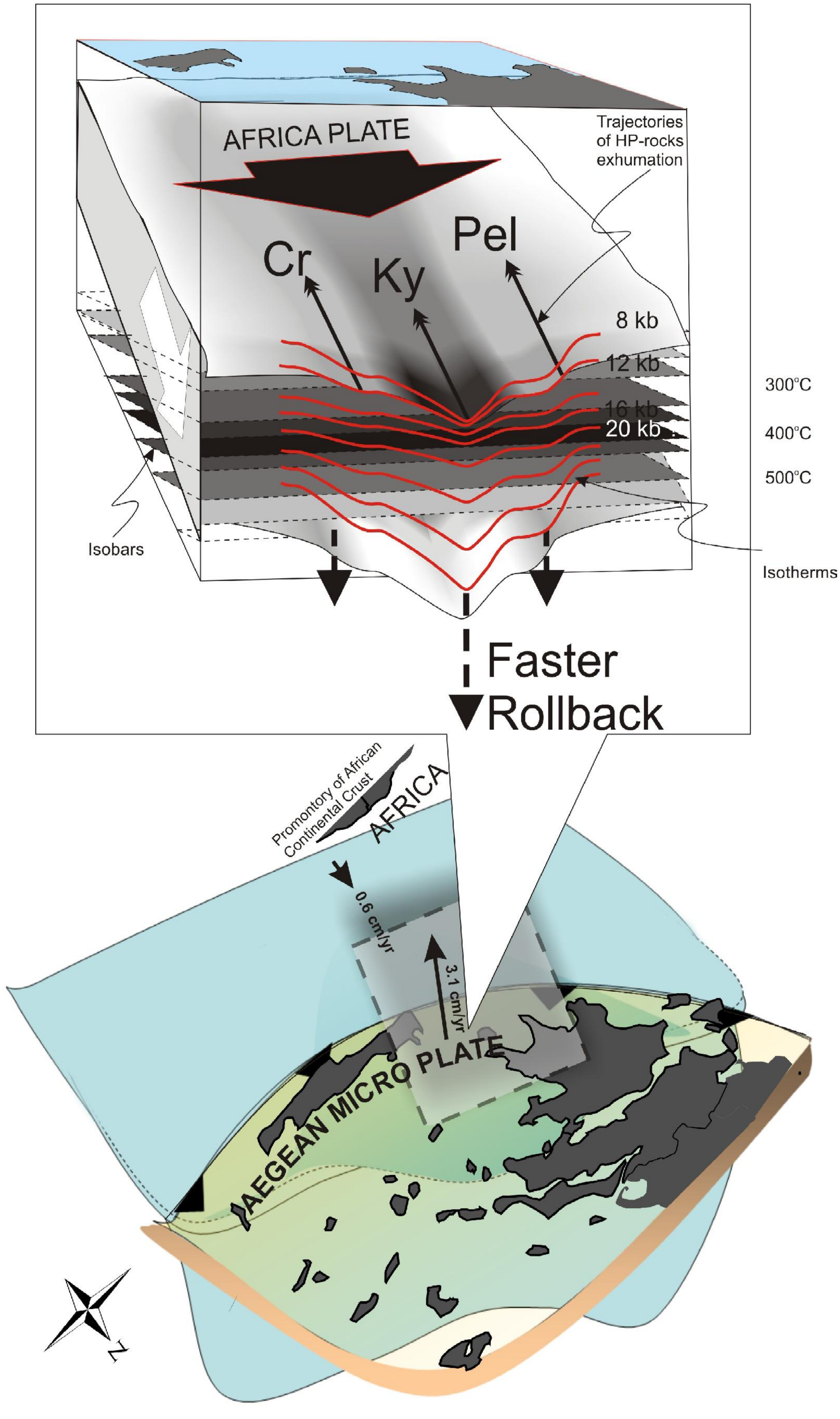
AFRICA PLATE
Trajectories of HP-rocks exhumation
Cr
Ky
Pel
8 kb
12 kb
16 kb
20 kb
300°C
400°C
500°C
Isobars
Isotherms
Faster Rollback
Promontory of African Continental Crust
AFRICA
0.6 cm/yr
3.1 cm/yr
AEGEAN MICRO PLATE
N

Figure 12 *(previous page)*: Depiction of the bending of isotherms during the bending of the subducting slab below the western half of the Hellenic forearc. GPS velocities derived from an average of five stations LEON, KYRA, OMAL, XRIS and ROML after McClusky et al., (2000).

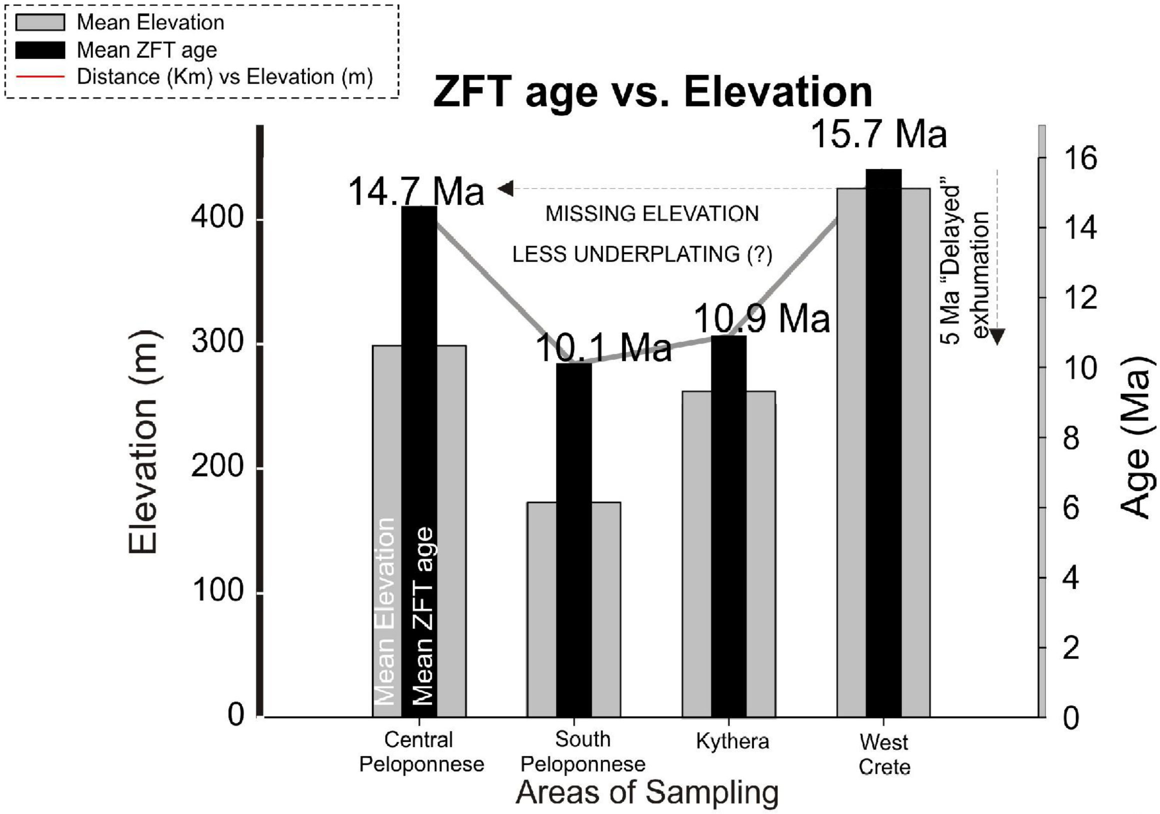

Mean Elevation
Mean ZFT age
Distance (Km) vs Elevation (m)
ZFT age vs. Elevation
15.7 Ma
14.7 Ma
MISSING ELEVATION
LESS UNDERPLATING (?)
10.1 Ma
10.9 Ma
5 Ma "Delayed" exhumation
Elevation (m)
Age (Ma)
Mean Elevation
Mean ZFT age
Central Peloponnese
South Peloponnese
Kythera
West Crete
Areas of Sampling

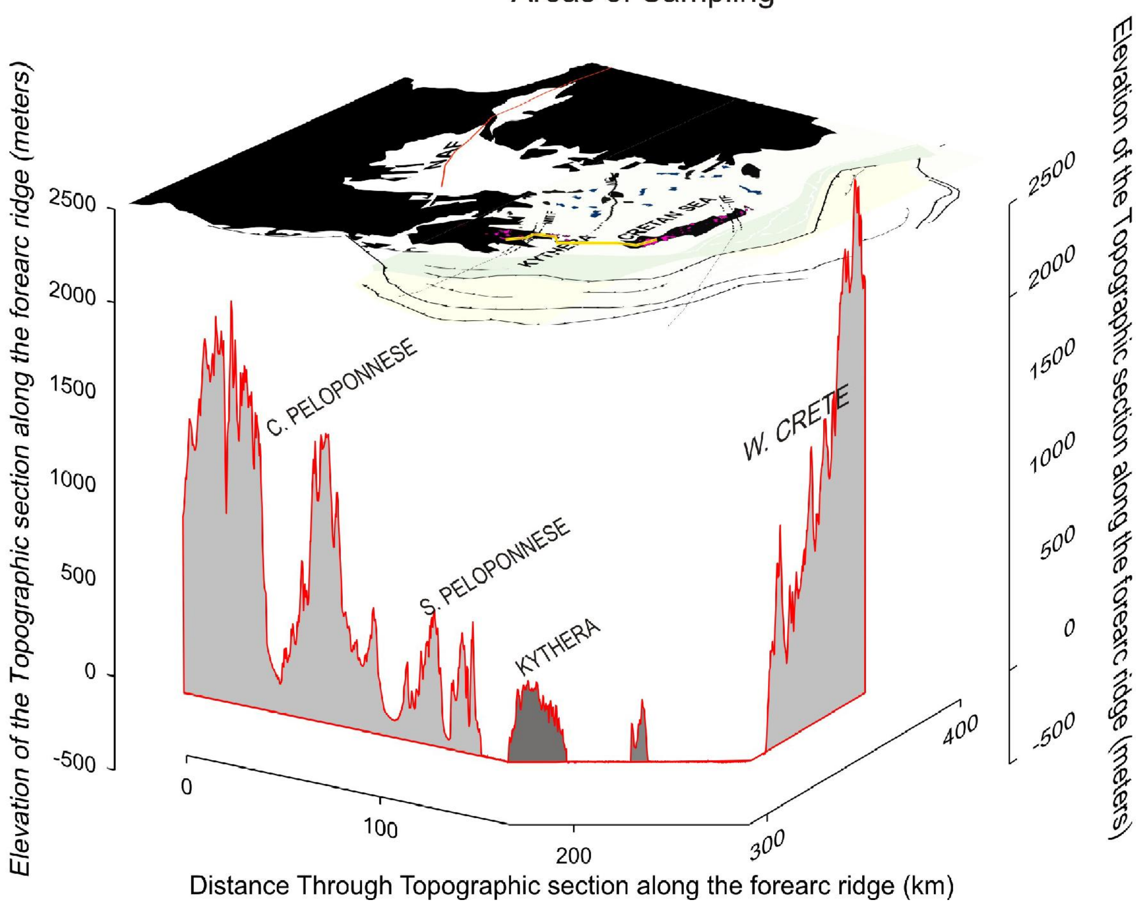

Elevation of the Topographic section along the forearc ridge (meters)
C. PELOPONNESE
S. PELOPONNESE
KYTHERA
W. CRETE
CRETAN SEA
Distance Through Topographic section along the forearc ridge (km)

Figure 13 *(previous page)*: The grey bars represent the mean elevation derived from the sample collection locations from each area. The black bars represent the mean ZFT age from all the samples of each individual area derived by the Binomfit program. The red line is the topographic profile along the forearc ridge through the sample locations.

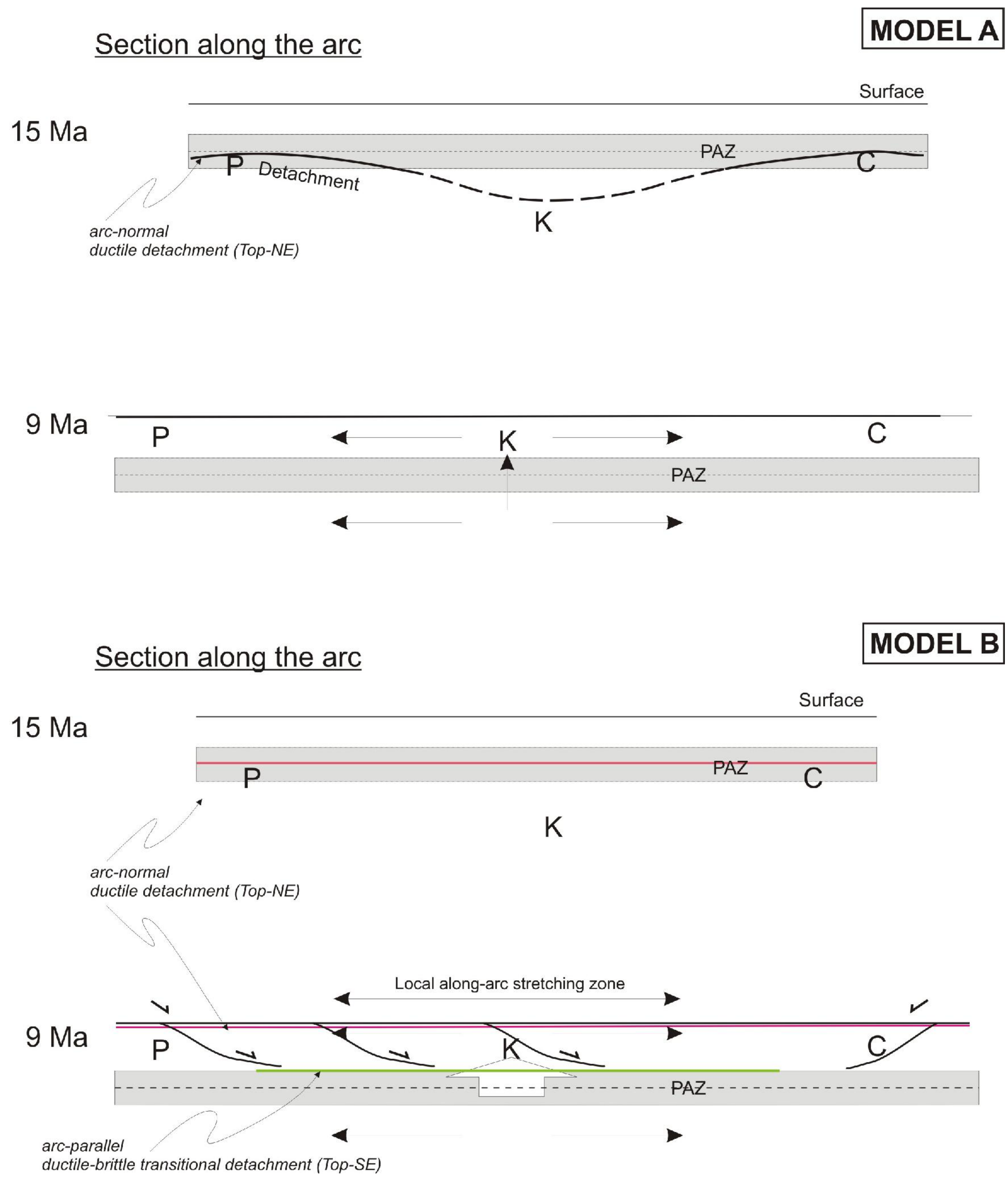

Figure 14: Two end-member hypothesis proposed shown in models A and B. In both models, Kythera PQU rocks are left at a lower crustal level after the first (arc-normal extension) stage but in model B the detachment is not held at depth. The rocks with older exhumation ages (central Peloponnese PQU and Crete PQU) are crossing the zircon PAZ (Partial Annealing Zone), while the rocks with younger exhumation ages (southeastern Peloponnese PQU and Kythera PQU) were deeper, below the PAZ. After 12 Ma the Kythera-Neapolis rocks are crossing the zircon PAZ faster than those of central Peloponnese and Crete.

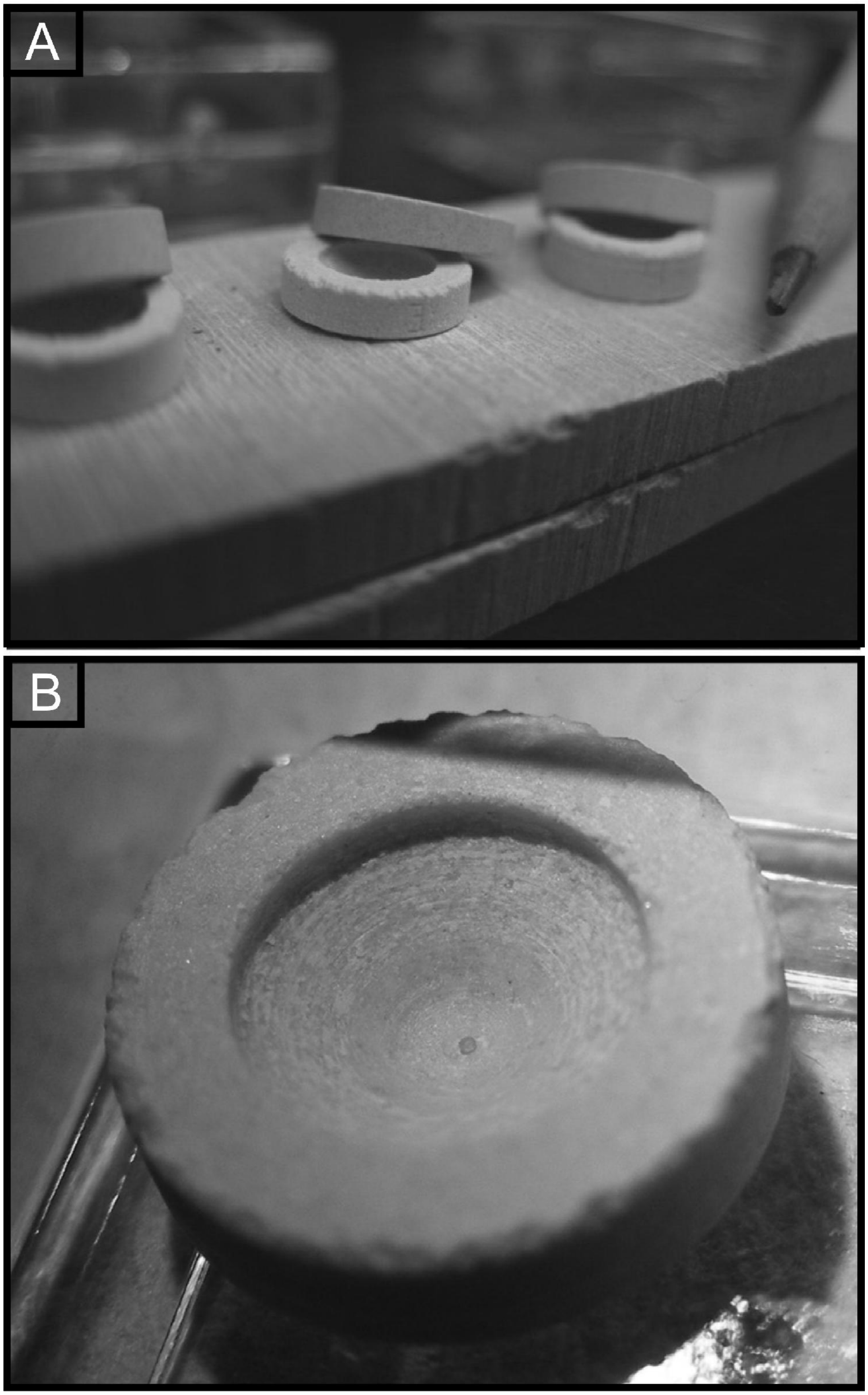

Figure 1: A. Pyrophyllite cases used for annealing individual zircon grains; B. One pyrophyllite case with a zircon of 130 μm length (c-axis) in the center.

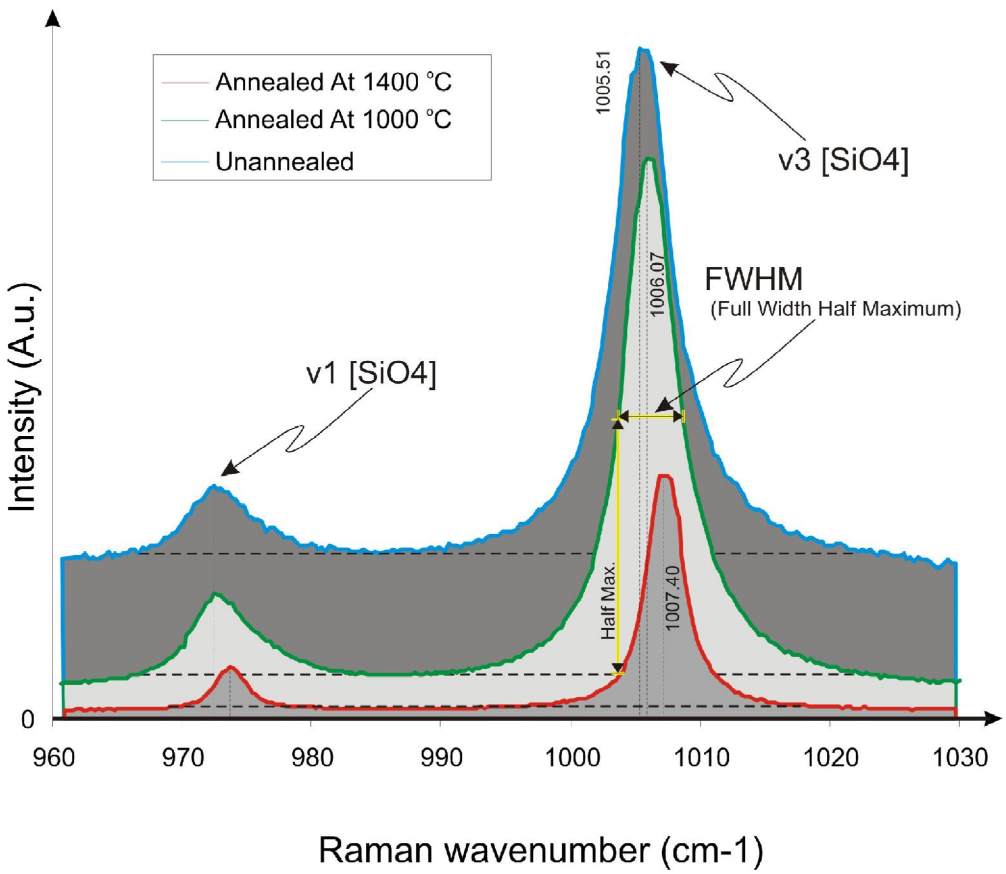

Figure 2: General band assignment for the most intense bands. FWHM stands for Full Width Half Maximum. The depicted Raman spectra belong to a zircon measured before annealing, and after two successive steps of annealing.

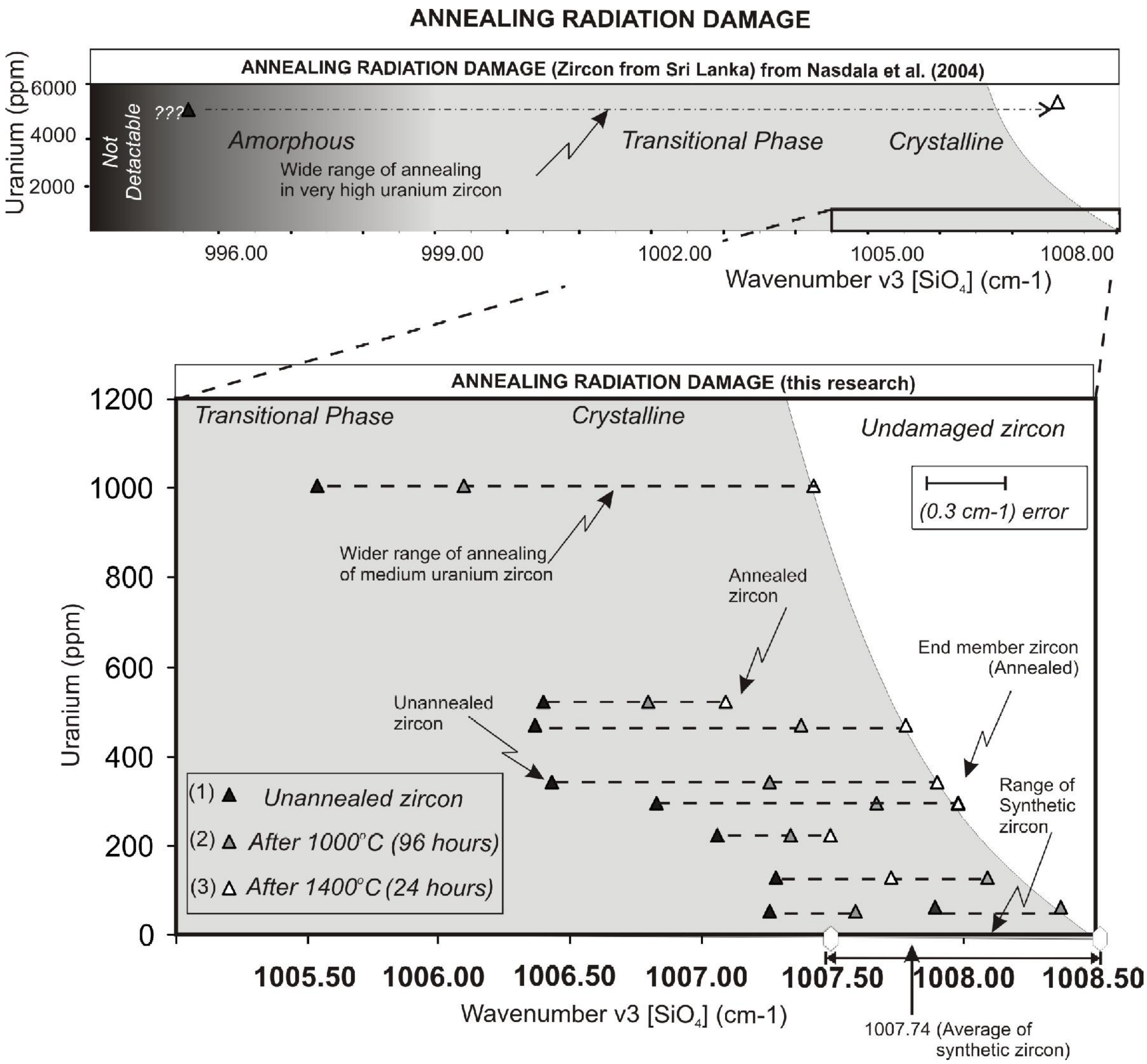

Figure 3: Raman measurements made on the same grains before and after 1000°C (96h) and 1400°C (24h) annealing experiments indicate that high-uranium concentration zircons show larger shift to higher wavenumbers than the low-uranium zircons. All move substantially towards the region of the synthetic zircons having no uranium content, and no radiation damage (the undamaged zircon region).

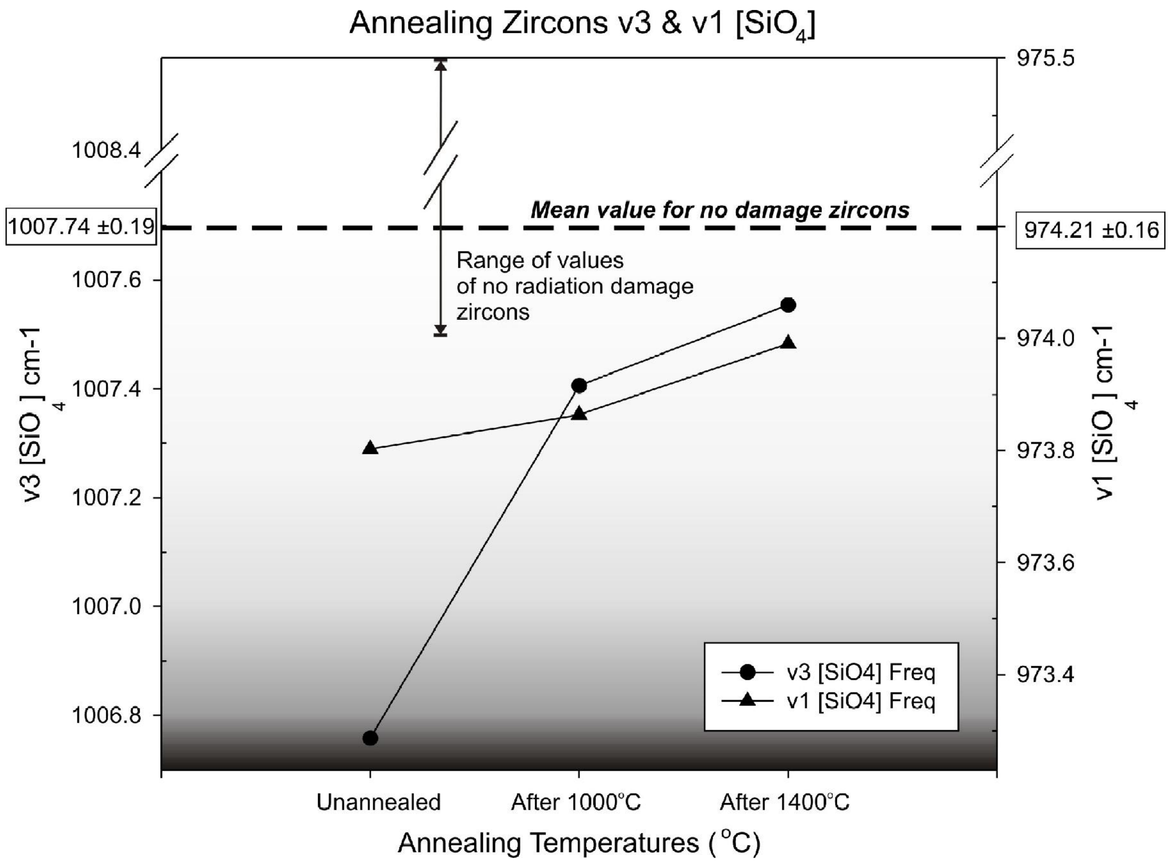

Figure 4: The average (3 measurements for first annealing and 5 measurements for second annealing) of the v3 and v1 frequencies of the annealed zircons. Those approach the end member zircon wavenumber range. Numbers in boxes are the v3 and v1 band frequencies of the synthetic zircons with no hafnium and no uranium content (and therefore no radiation damage) with their standard deviation.

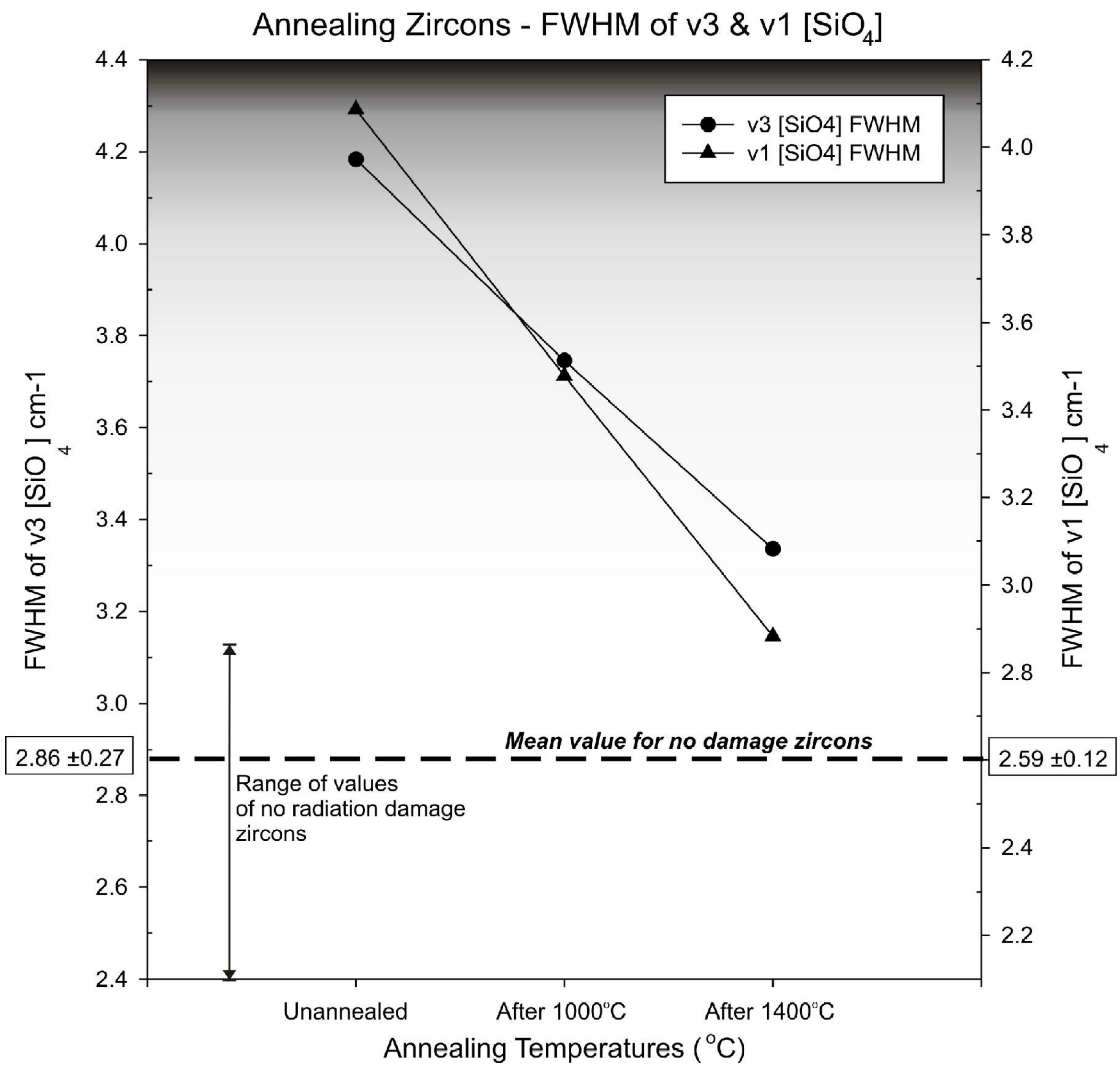

***Figure* 5**: The average of the FWHM of the v3 and v1 Raman spectra only approach the undamaged zircon wavenumber range implying less than full annealing or an annealing process which does not directly invert progressive metamictization. Numbers in boxes are the FWHM of v3 and v1 band frequencies of the synthetic zircons of no hafnium and no uranium content, (and therefore no radiation damage) with their standard deviation.

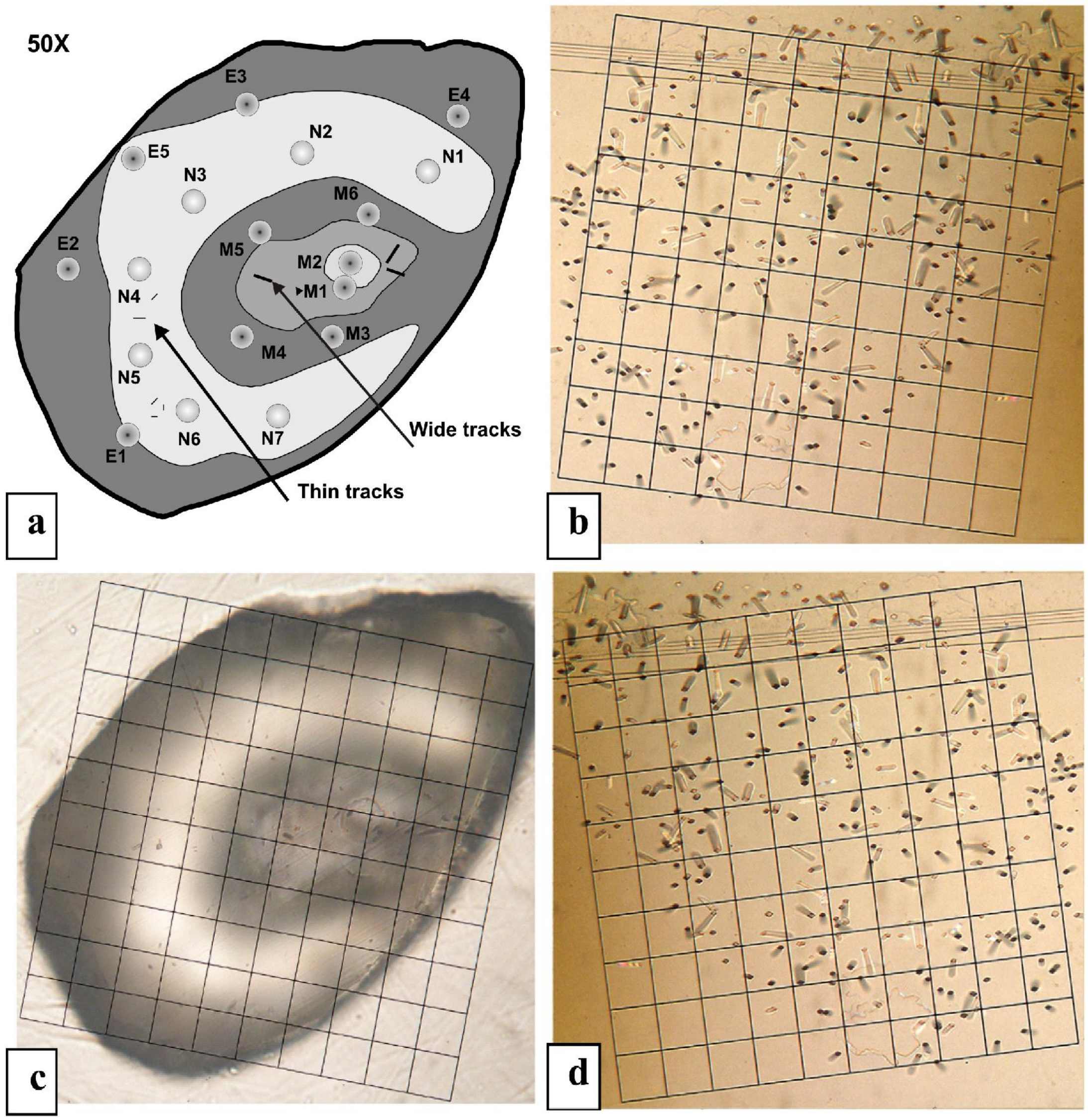

Figure 6: (a) Grain map of Raman analysis locations for a zoned zircon grain; (b) figure 6d flipped horizontally to match the orientation of the diagram in (a); (c) photomicrograph of the zircon under plane transmitted light (50x objective); (d) mica print of the zircon after irradiation showing the induced fission tracks in the mica.

#	v3 [SiO4] (cm-1)	#	v3 [SiO4] (cm-1)	#	V3 [SiO4] (cm-1)
M1	1006.84	N1	1007.12	E1	1006.69
M2	1006.84	N2	1007.12	E2	1006.97
M3	1006.84	N3	1007.12	E3	1006.97
M4	1006.84	N4	1007.12	E4	1006.97
M5	1006.84	N5	1007.12	E5	1007.26
M6	1007.12	N6	1007.70		
		N7	1007.26		

***Table 1*:** Raman data of the v3 [SiO4] band from the zircon of Fig. 6.

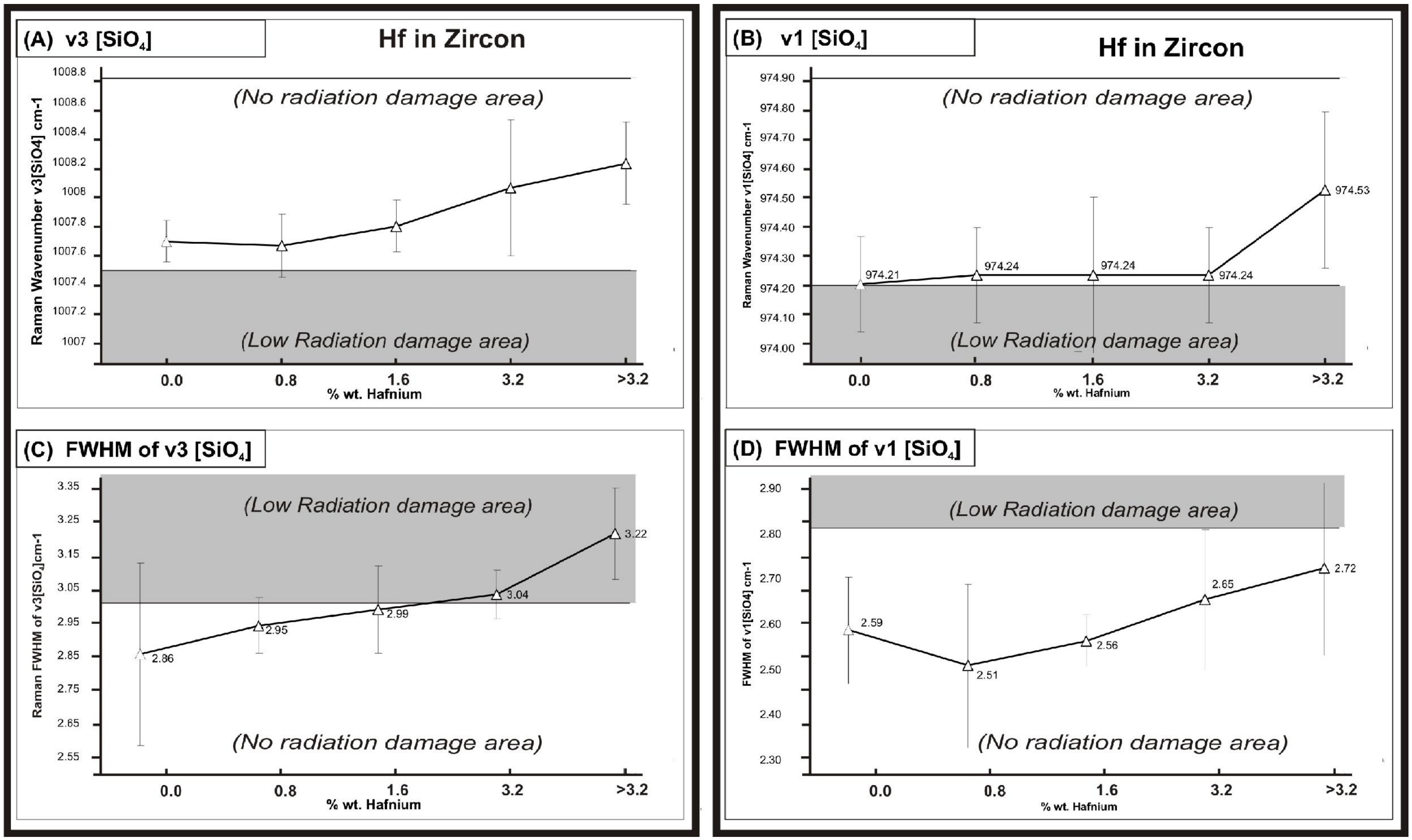

***Figure** 7*: Raman spectra measurements of the v3 and v1 [SiO_4] peak wavenumber, as well as their FWHM, of the synthetic zircons, with and without hafnium content, versus the zircon uranium concentration. Error bars represent are standard deviation.

Table 2: Raman wavenumber frequencies of v1 and v3 [SiO_4] bands and their FWHM for the synthetic zircons, with and without hafnium content.

Synthetic Zircon grains**	Hf (wt%)	U (wt%)	Freq. of v3 [SiO_4] (cm-1)	STDEV* of v3 [SiO_4]	FWHM of v3 [SiO_4]	STDEV* of v3 FWHM	Freq. of v1 [SiO_4] (cm-1)	STDEV* of v1 [SiO_4]	FWHM of v1 [SiO_4]	STDEV* of v1 FWHM
57	*0*	0	**1007.74**	0.19	**2.86**	0.27	**974.21**	0.16	**2.59**	0.12
5	*0.8*	0	**1007.71**	0.15	**2.95**	0.08	**974.24**	0.16	**2.51**	0.18
5	*1.6*	0	**1007.83**	0.40	**2.99**	0.13	**974.24**	0.26	**2.56**	0.06
5	*3.2*	0	**1008.05**	0.24	**3.04**	0.07	**974.24**	0.16	**2.65**	0.16
15	*> 3.2*	0	**1008.20**	0.26	**3.22**	0.14	**974.53**	0.26	**2.72**	0.19

Note: *STDEV stands for standard deviation.

**Synthetic zircons have no uranium and no radiation damage. >3.2: those 15 zircon grains have an undefined Hf (wt%) concentration, and considering the v3 frequency may have higher Hf wt% than the five grains of 3.2 wt% Hf.

FWHM stands for Full Width Half Maximum.

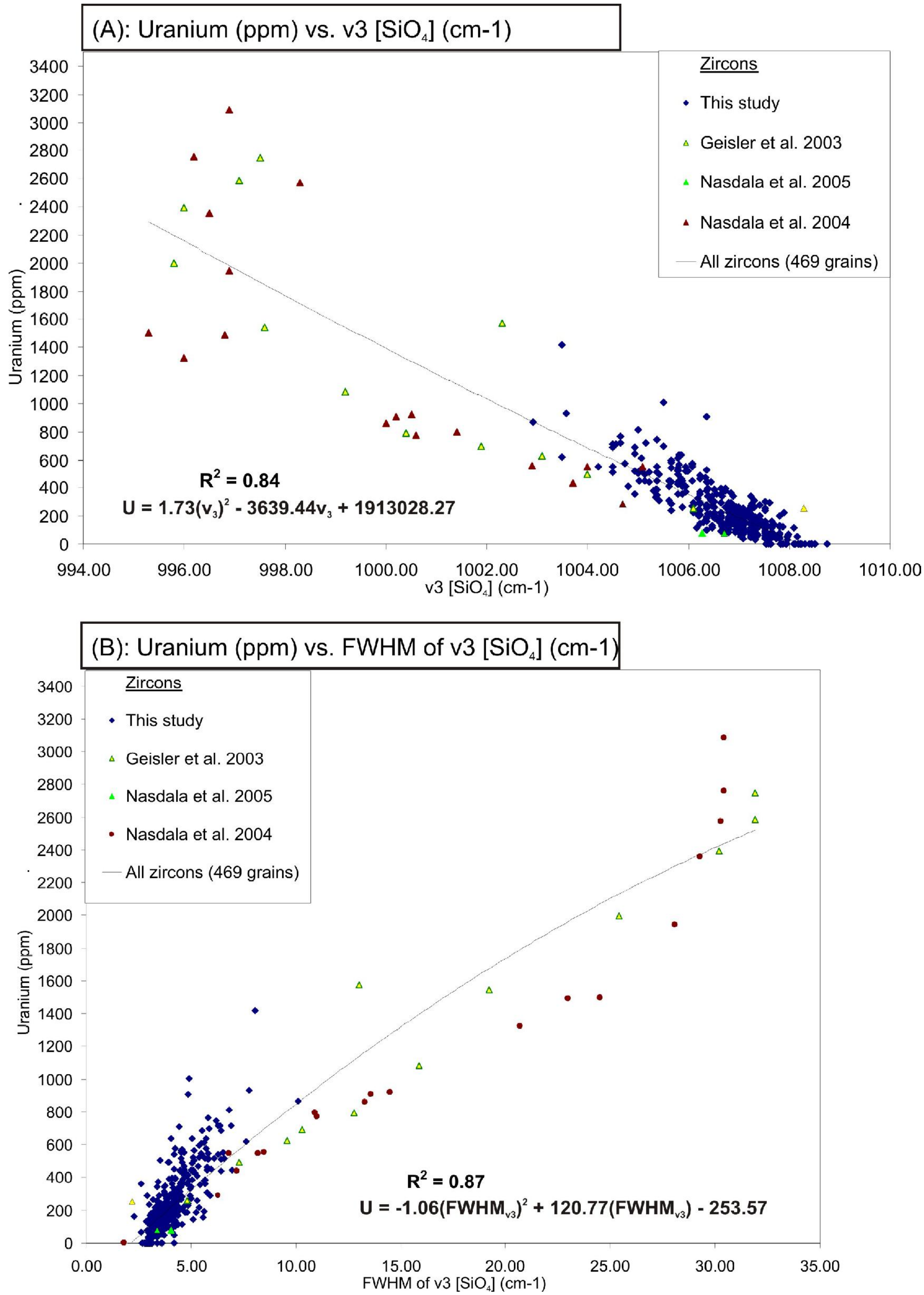

Figure 8: (A) High correlation between the Raman wavenumber of the v3 [SiO_4] band frequencies, and (B) Full Width Half Maximum - FWHM of the v3 [SiO_4] band peak plotted against the uranium content of individual natural zircons.

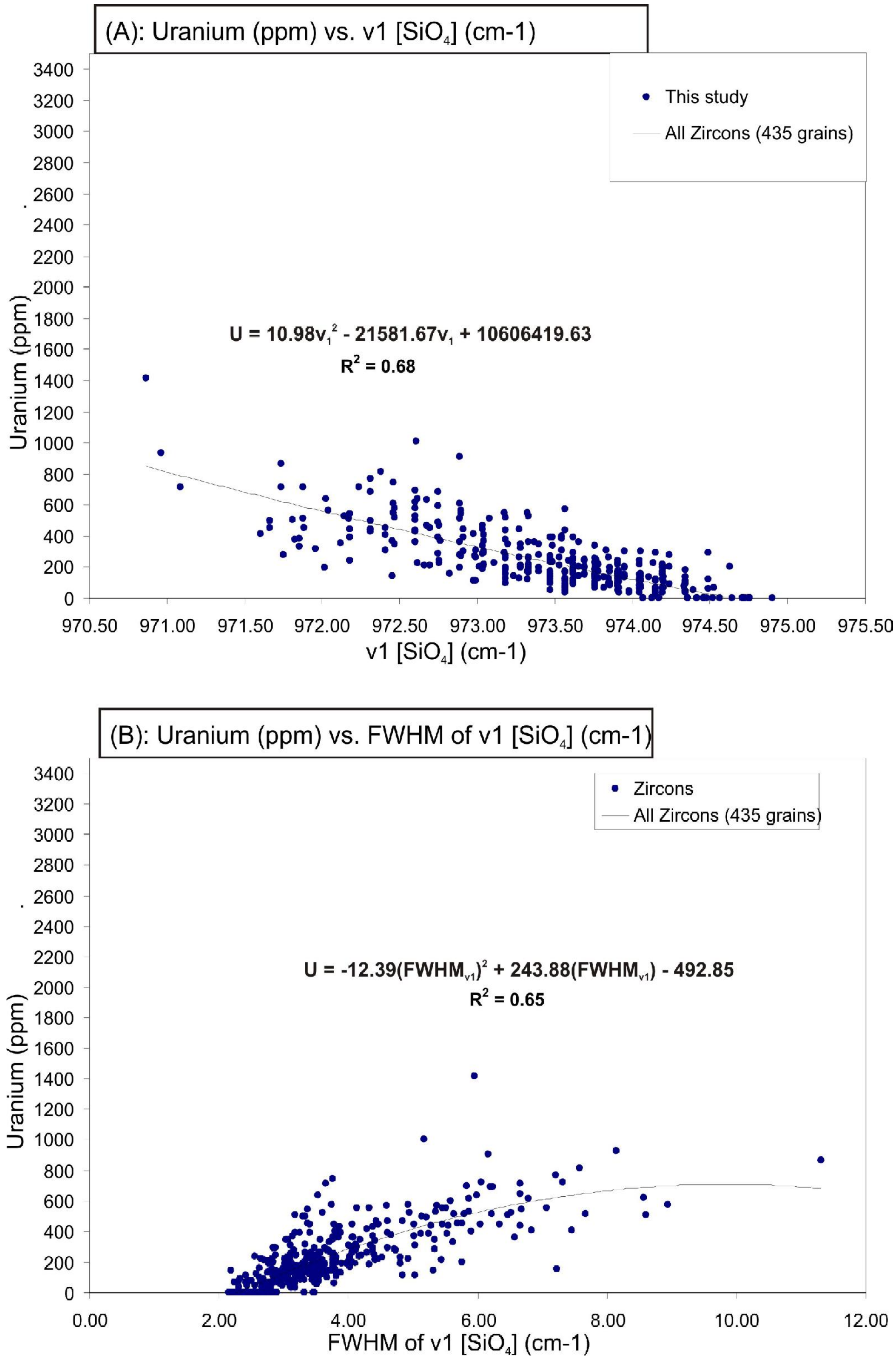

Figure 9: Correlation between (A) the Raman wavenumber of the v1 [SiO_4] band frequencies and (B) FWHM of v1 [SiO_4] band peak, and uranium content of individual natural zircons.

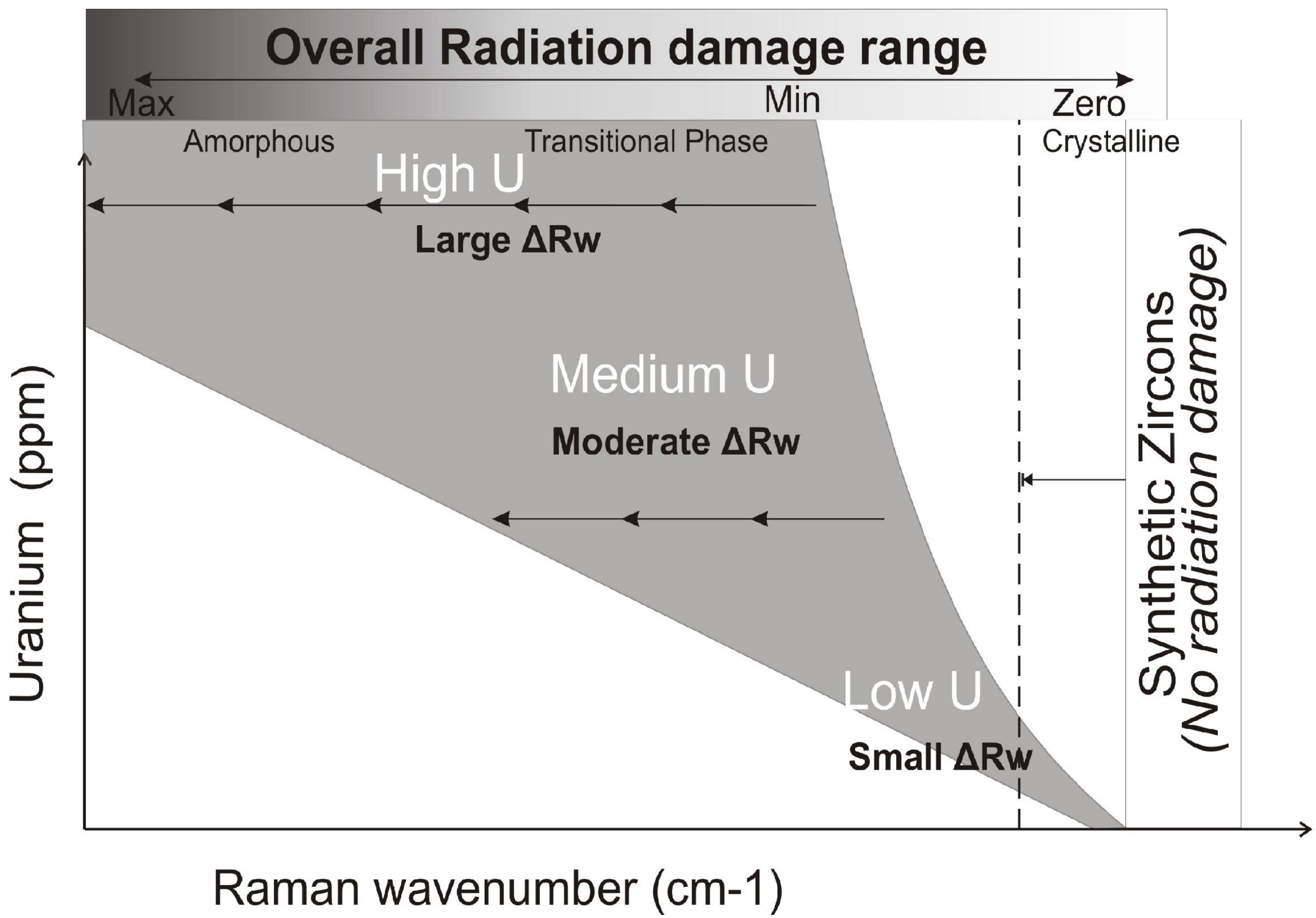

Figure 10: Raman wavenumber range increases with uranium concentration, reflecting the degree of saturation of the zircon by accumulated radiation damage (the proportion of the distorted to undistorted crystallinity in zircon).

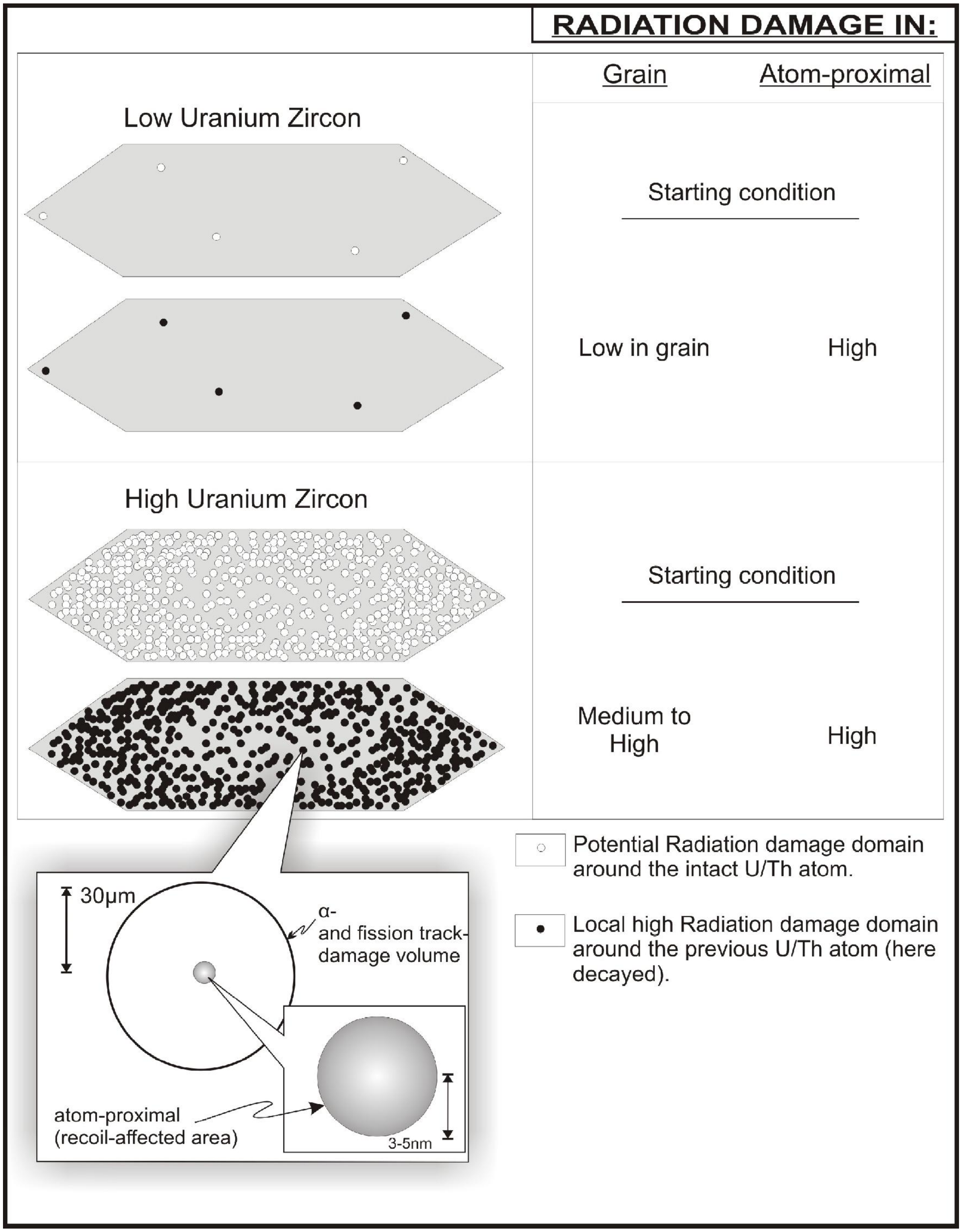

Figure 11: Radiation damage over same elapsed time in low- and high-U,Th concentration zircon. The radiation damage in the recoil-affected area around the daughter atom as well as the entire crystallinity of the zircon depends on the uranium/thorium content in the grain. Low U,Th content results in a small number of alpha, recoil and fission events, in the zircon host, and a low volume of overall radiation damage. In contrast, natural high-uranium zircon results in a much denser distribution of radiation damage compared to low-uranium zircon.

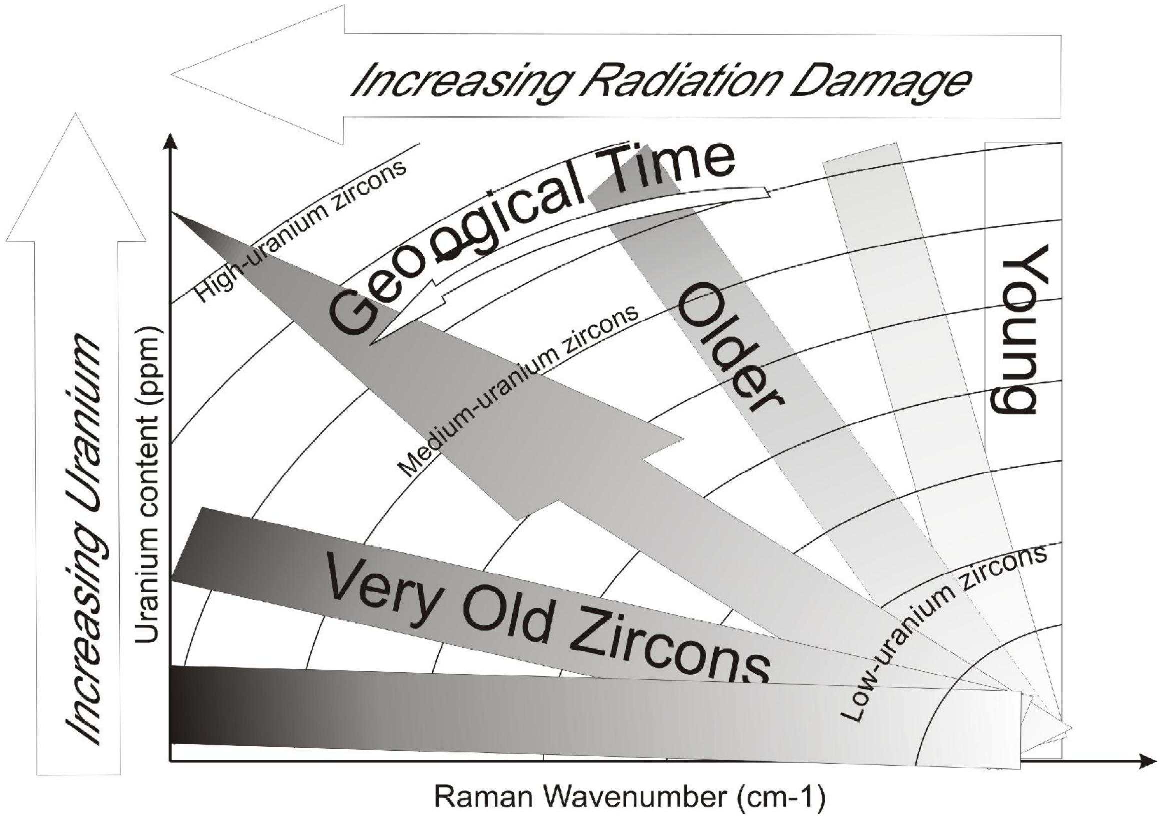

Figure 12: Low-uranium zircon needs a long time to approach the same amount of decay events of a high-uranium zircon to show equal apparent radiation damage. Time is what distinguishes zircons of same uranium concentration in the apparent radiation damage range. The radiation damage range indicated by Raman wavenumber shift may allow development of a new chronometer using Raman measurements.